Published in final edited form as:

Cell. 2022 May 26; 185(11): 1943–1959.e21. doi:10.1016/j.cell.2022.04.020.

PAAN/MIF nuclease inhibition prevents neurodegeneration in Parkinson's disease

Hyejin Park[1,2,7], **Tae-In Kam**[1,2,3,7], **Hanjing Peng**[4], **Shih-Ching Chou**[1,4], **Amir A. Mehrabani-Tabari**[1], **Jae-Jin Song**[1,2], **Xiling Yin**[1,2], **Senthilkumar S. Karuppagounder**[1,2], **George K. Umanah**[1,2], **A.V. Subba Rao**[4], **YuRee Choi**[1,2], **Akanksha Aggarwal**[1], **Sohyun Chang**[1], **Hyunhee Kim**[1], **Jiyoung Byun**[1], **Jun O. Liu**[4], **Ted M. Dawson**[1,2,3,4,5,8,9,*], **Valina L. Dawson**[1,2,3,5,6,8,*]

[1]Neuroregeneration and Stem Cell Programs, Institute for Cell Engineering, Johns Hopkins University School of Medicine, Baltimore, MD 21205, USA

[2]Department of Neurology, Johns Hopkins University School of Medicine, Baltimore, MD 21205, USA

[3]Adrienne Helis Malvin and Diana Helis Henry Medical Research Foundation, New Orleans, LA 70130-2685, USA

[4]Department of Pharmacology and Molecular Sciences and SJ Yan and HJ Mao Laboratory of Chemical Biology, Johns Hopkins University School of Medicine, Baltimore, MD 21205, USA

[5]Solomon H. Snyder Department of Neuroscience, Johns Hopkins University School of Medicine, Baltimore, MD 21205, USA

[6]Department of Physiology, Johns Hopkins University School of Medicine, Baltimore, MD 21205, USA

[7]These authors contributed equally

[8]These authors contributed equally

[*]Correspondence: tdawson@jhmi.edu (T.M.D.), vdawson@jhmi.edu (V.L.D.).

AUTHOR CONTRIBUTIONS

Conceptualization, H. Park, T.-I.K., T.M.D., and V.L.D.; methodology, H. Park, T.-I.K., H. Peng, S.C.C., J.-J.S., X.Y., A.A.M.-T., S.S.K., G.K.U., A.V.S.R., Y.C., A.A., S.C., H.K., and J.B.; validation, H. Park, T.-I.K., S.C.C., J.-J.S., A.A.M.-T., X.Y., and S.S.K.; formal analysis, H. Park, T.-I.K., S.C.C., J.-J.S., X.Y., and S.S.K.; investigation, H. Park, T.-I.K., H. Peng, J.-J.S., X.Y., A.A.M.-T., S.S.K., G.K.U., A.V.S.R., Y.C., A.A., S.C., H.K., and J.B.; resources, H. Park, T.-I.K., H. Peng, J.O.L., T.M.D., and V.L.D.; writing—original draft, H. Park, T.-I.K., T.M.D., and V.L.D.; visualization, H. Park and T.-I.K.; supervision, T.M.D. and V.L.D.; funding acquisition, T.M.D. and V.L.D.

DECLARATION OF INTERESTS

H. Park, T.-I.K., H. Peng, A.V.S.R., J.O.L., T.M.D., and V.L.D. are inventors of technology discussed in this this publication, which Neuraly is in the process of licensing from Johns Hopkins University. T.M.D. and V.L.D. are founders of Neuraly and hold shares of stock options as well as equity in Neuraly, which is a subsidiary of D & D Pharmatech. This arrangement has been reviewed and approved by Johns Hopkins University in accordance with its conflict-of-interest policies. Patent applications covering the rapafucin library have been filed by Johns Hopkins University and licensed to Rapafusyn Pharmaceuticals. J.O.L. is a co-founder of, as well as a Scientific Advisory Board Member for, Rapafusyn Pharmaceuticals. This arrangement has been reviewed and approved by the Johns Hopkins University in accordance with its conflict-of-interest policies.

INCLUSION AND DIVERSITY

For studies involving non-human subjects or material, We worked to ensure sex balance in the selection of non-human subjects.

SUPPLEMENTAL INFORMATION

Supplemental information can be found online at https://doi.org/10.1016/j.cell.2022.04.020.

[9]Lead contact

SUMMARY

Parthanatos-associated apoptosis-inducing factor (AIF) nuclease (PAAN), also known as macrophage migration inhibitor factor (MIF), is a member of the PD-D/E(X)K nucleases that acts as a final executioner in parthanatos. PAAN's role in Parkinson's disease (PD) and whether it is amenable to chemical inhibition is not known. Here, we show that neurodegeneration induced by pathologic α-synuclein (α-syn) occurs via PAAN/MIF nuclease activity. Genetic depletion of PAAN/MIF and a mutant lacking nuclease activity prevent the loss of dopaminergic neurons and behavioral deficits in the α-syn preformed fibril (PFF) mouse model of sporadic PD. Compound screening led to the identification of PAANIB-1, a brain-penetrant PAAN/MIF nuclease inhibitor that prevents neurodegeneration induced by α-syn PFF, AAV-α-syn overexpression, or MPTP intoxication *in vivo*. Our findings could have broad relevance in human pathologies where parthanatos plays a role in the development of cell death inhibitors targeting the druggable PAAN/MIF nuclease.

In brief

Neurodegeneration in Parkinson's disease occurs via PAAN/MIF nuclease activity and is amenable to inhibition with a brain-penetrant small molecule inhibitor.

Graphical Abstract

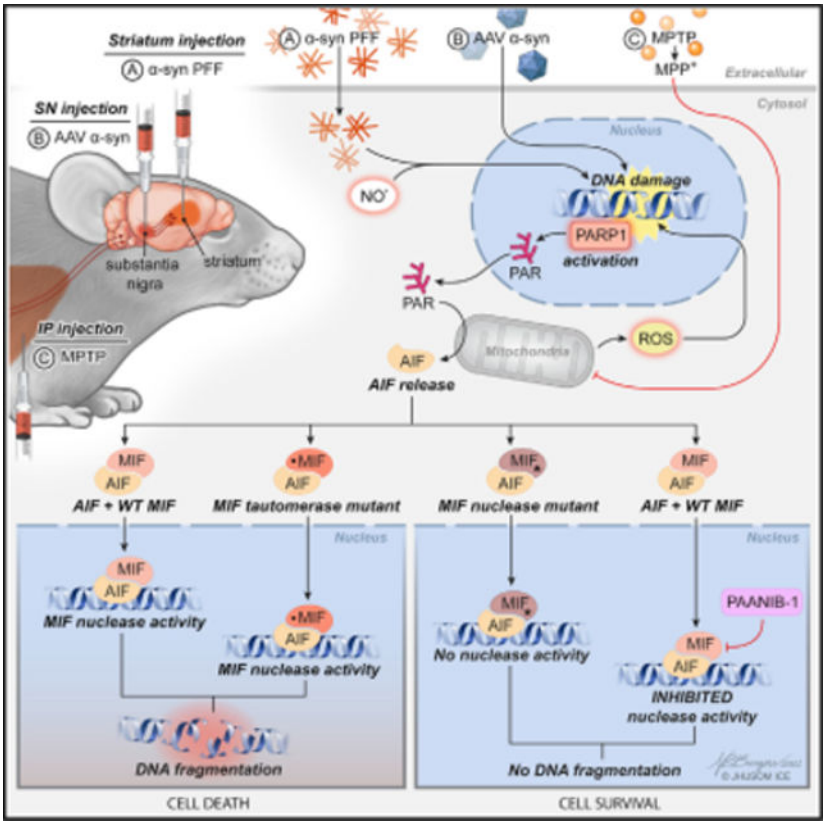

INTRODUCTION

Parkinson's disease (PD) is the most common neurodegenerative movement disorder in which intracellular α-synuclein (α-syn) aggregates into higher molecular pathologic structures that ultimately lead to neurodegeneration (Henderson et al., 2019). Pathologic α-syn-mediated neurodegeneration in PD occurs through parthanatos-dependent cell death through activation of poly(ADP-ribose) (PAR) polymerase-1 (PARP-1) (Kam et al., 2018; Lengyel-Zhand et al., 2022; Puentes et al., 2021). Despite the emerging role of PAR signaling in the pathogenesis of PD, chronic inhibition of PARP-1 as a disease-modifying therapy in PD may be perilous. PARP inhibitors would interfere with the myriad physiologic functions of PARP, which may have unintended consequences in a chronic disease (Berger et al., 2018). In addition, most if not all PARP inhibitors interfere with DNA repair by trapping PARP on DNA strand breaks (Zandarashvili et al., 2020), which provides synthetic lethality in the treatment of certain cancers (Lord and Ashworth, 2017). Interference with DNA repair could also create unforeseen toxicity in chronic neurodegenerative diseases.

The parthanatos-associated apoptosis-inducing factor (AIF) nuclease (PAAN) also known as macrophage migration inhibitor factor (MIF) was shown to be a major mediator of parthanatic cell death in acute disorders via its nuclease activity (Wang et al., 2016; Yang et al., 2020). MIF is also known to have tautomerase activity and to act as an atypical extracellular cytokine (Bloom et al., 2016; Fingerle-Rowson et al., 2009; Hermanowski-Vosatka et al., 1999; Metz and Bucala, 1997; Paralkar and Wistow, 1994; Rosengren et al., 1996). The identification of the enzymatic function for MIF as a member of the large PD-D/E(X)K nuclease superfamily brought to the forefront a role for MIF in cell death, in that its nuclease activity is responsible for the large-scale DNA fragmentation that occurs in parthanatos (Park et al., 2020; Wang and Ge, 2020; Wang et al., 2016; Zhou et al., 2021). Whether PAAN/MIF nuclease activity and/or its tautomerase activity plays a role in a chronic neurodegenerative disorder, such as PD is not known. Moreover, no PAAN/MIF nuclease-specific inhibitors exist. Here, we identify a PAAN/MIF inhibitor, PAANIB-1 and evaluated whether genetic and pharmacological inhibition of PAAN/MIF nuclease activity prevents neurodegeneration in mouse models of PD.

RESULTS

α-Syn PFF-induced pathology is reduced by deletion of PAAN/MIF or lack of PAAN/MIF's nuclease activity *in vivo*

To determine whether PAAN/MIF is essential for pathologic α-syn induced degeneration, recombinant α-synuclein preformed fibrils (PFFs) were stereotaxically injected into the striatum of wild type (WT) and PAAN/MIF knockout (KO) mice (Bozza et al., 1999). As previously described (Luk et al., 2012; Mao et al., 2016), WT mice showed an approximate 50% loss of dopamine (DA) neurons 6 months after a single intrastriatal injection of α-syn PFF (Figures 1A and 1B). In contrast, injection of α-syn PFF failed to induce DA cell loss in PAAN/MIF KO mice (Figures 1A and 1B). Tyrosine hydroxylase (TH) and dopamine transporter (DAT) levels were also reduced in WT mice in response to α-syn PFF as determined by western blot analysis, while the reduction in TH and DAT levels is prevented in PAAN/MIF-deficient mice (Figures S1A and S1B). Accompanying the loss of

DA neurons was a reduction in striatal DA and its metabolites, 3,4-dihydroxyphenylacetic acid (DOPAC) as determined by high-performance liquid chromatography (HPLC) in α-syn PFF-injected WT mice, but not in PAAN/MIF KO mice (Figures 1C and 1D). Striatal α-syn PFF significantly increased the DA turnover in WT mice, whereas these effects were attenuated in PAAN/MIF KO mice (Figures S1C and S1D). The absence of PAAN/MIF prevented the α-syn PFF-induced behavioral deficits on the hindlimb clasping test (Figure S1E), pole test (Figure 1E), and grip strength test (Figure 1F). Taken together, these results indicate that the striatal α-syn PFF-induced loss of DA neurons is dependent on PAAN/MIF.

PAAN/MIF was originally identified as an atypical secreted cytokine (Bucala, 1996) that exhibits tautomerase activity that accounts for some but not all of MIF's pleiotropic actions (Bloom et al., 2016; Fingerle-Rowson et al., 2009; Hermanowski-Vosatka et al., 1999; Metz and Bucala, 1997; Paralkar and Wistow, 1994; Rosengren et al., 1996). When PAAN/MIF is recruited to the nucleus under stress conditions, it acquires a gain of function activity as a nuclease. Its nuclease activity is distinct from its actions as a cytokine and tautomerase (Park et al., 2020; Wang et al., 2016). Accordingly, the relative contribution of PAAN/MIF's nuclease activity versus MIF's tautomerase activity in pathologic α-syn-induced degeneration was evaluated. Mice lacking PAAN/MIF nuclease activity (MIF E22Q) were resistant to α-syn PFF-induced neurodegeneration, while mice lacking MIF's tautomerase activity (MIF P2G) (Fingerle-Rowson et al., 2009) were as sensitive as WT mice in α-syn PFF-induced neurodegeneration as assessed by stereologic counting of TH immunoreactivity (Figures 1G and 1H) and Nissl staining (Figures 1G and S1F), immunoblot analysis of TH levels (Figures S1G and S1H), HPLC assessment of DA (Figure 1I), and its metabolite, DOPAC levels (Figure S1I), DA turnover (Figures S1J and S1K) and the accompanying behavioral deficits including pole test (Figure 1J) and grip strength test (Figure 1K). Consistent with previous reports that indicate that loss of SNpc DA neurons occurs 6 months after α-syn PFF injection, but not at earlier time point (Kam et al., 2018; Luk et al., 2012), pulse gel electrophoresis indicates that genomic DNA cleavage primarily coincides with the loss of DA neurons since there is no genomic DNA cleavage 1 and 3 months after α-syn PFF injection (Figure S1L). α-syn PFF induces genomic DNA cleavage in the substantia nigra of WT and MIF P2G mice 6 months after the α-syn PFF injection, while it is significantly attenuated in PAAN/MIF E22Q mice (Figures 1L and 1M). Viral transgenesis of adeno-associated viral (AAV) expression of PAAN/MIF WT, PAAN/MIF E22Q, and MIF P2G in MIF KO mice further confirmed that PAAN/MIF's nuclease activity, but not MIF's tautomerase activity, is required for α-syn PFF-induced neurodegeneration *in vivo* (Figures S2A–S2H).

Nuclear translocation of PAAN/MIF nuclease mediates α-syn PFF-induced genomic DNA cleavage and neuronal death

To further evaluate the PAAN/MIF nuclease versus it tautomerase activity in α-syn PFF toxicity, primary neuronal cultures were utilized as previously described (Kam et al., 2018; Mao et al., 2016). α-syn PFF induced nuclear translocation of PAAN/MIF and AIF that was attenuated by the poly (ADP-ribose) polymerase (PARP) inhibitor, ABT-888 (Figure 2A). In addition, treatment of AP5 or 2,3-dioxo-6-nitro-7-sulfamoyl-benzo[f]quinoxaline (NBQX), selective NMDA or AMPA receptor antagonists, respectively, inhibited α-syn

PFF-induced PARP activation (Figure S3A) and thereby attenuated the nuclear translocation of AIF and MIF (Figure S3B). These results are consistent with prior reports suggesting that glutamate-related neuronal activity regulates cell-to-cell propagation of pathologic α-syn (Ueda et al., 2021; Yamada and Iwatsubo, 2018). Co-immunoprecipitation indicates that AIF and PAAN/MIF interact following α-syn PFF administration (Figure 2B) and they co-localize in the nucleus (Figure 2C). There was no difference in nuclear translocation of PAAN/MIF WT, E22Q, and MIF P2G in response to α-syn PFF (Figure S3C). Knockout of PAAN/MIF prevented α-syn PFF-induced cleavage of genomic DNA (Figure 2D), cell death (Figures 2E and 2F), and accumulation of insoluble phosphorylation of α-syn on Serine129, a marker of pathologic α-syn (Fujiwara et al., 2002) (Figures S3D and S3E) in neuronal cultures. Cleavage of genomic DNA and cell death in response to α-syn PFF were restored by lentiviral expression of PAAN/MIF WT and MIF P2G in MIF KO neuronal cultures but were still attenuated in KO neurons transduced with PAAN/MIF E22Q and the AIF binding deficient mutant PAAN/MIF E22A (Figures 2D–2F). Similar results were obtained in PAAN/MIF E22Q and MIF P2G knock in neuronal cultures (Figures 2G and 2H). These data indicate that PAAN/MIF's nuclease activity and its binding to AIF is required for cleavage of genomic DNA and cell death induced by α-syn PFF. MIF also acts as an extracellular cytokine that counter regulates the glucocorticoid TNF-α elevation (Calandra et al., 1995; Flaster et al., 2007; Roger et al., 2005). PAAN/MIF WT, PAAN/MIF E22Q, and MIF P2G are equally effective in preventing dexamethasone, a synthetic glucocorticoid, inhibition of TNF-α production (Figure S3F). α-Syn PFF induced extracellular secretion is equivalent between PAAN/MIF WT, PAAN/MIF E22Q, and MIF P2G (Figure S3G). Thus, PAAM/MIF E22Q or MIF P2G do not seem to have a substantial effect on MIF's ability to act as a cytokine. D-dopachrome tautomerase (D-DT or MIF-2), a member of the MIF protein superfamily that functions as a MIF-like cytokine but does not have an E22 residue that is critical for PAAN/MIF's nuclease activity (Merk et al., 2011), did not have nuclease activity (Figure S3H). Together, these results strongly suggest that the nuclease, but not the tautomerase or cytokine, activity of PAAN/MIF is required for α-syn PFF-induced neurodegeneration.

Identification of the PAAN/MIF nuclease inhibitors

Since there are no PAAN/MIF nuclease inhibitors, we developed an assay to screen for PAAN/MIF nuclease inhibitors. Single-stranded PAAN/MIF nuclease DNA substrate (Wang et al., 2016) was amine modified on the 5' end and immobilized on a plate. Hybridization with a biotin-labeled complementary oligonucleotide followed by addition of streptavidin-conjugated horseradish peroxidase enzyme (HRP) leads to retention of HRP on the surface within each well in the presence of intact PAAN/MIF nuclease DNA substrate, which can be quantitatively detected through colorimetric change at 450 nm using the HRP substrate 3,3′,5,5′-tetramethylbenzidine (TMB). In the presence of WT PAAN/MIF, there is reduced signal, indicative of cleavage of the PAAN/MIF nuclease substrate, while the signal is not attenuated without recombinant PAAN/MIF (Figures 3A and S4A). The rapamycin-inspired macrocycle library, known as the rapafucins, bearing a conserved FK506-binding protein (FKBP)-binding domain, and a variable tetrapeptide effector domain was recently developed and shown to possess enhanced target specificity and pharmacological activity (Guo et al., 2019b). Thus, the rapafucin library containing 45,000 macrocyclic compounds in 3,000

pools of 15 compounds was screened using this assay. The Z′ factors were within the 0.5–1 range, indicating that minimal variations within days and between plates were observed (Figure S4B). Several pools were identified that inhibit PAAN/MIF nuclease activity from the primary screen (Figure 3B). Pools that inhibited PAAN/MIF nuclease *in vitro* by at least 60% were rescreened for both inhibition of PAAN/MIF nuclease activity and prevention of parthanatic cell death induced by 50-μM *N*-Methyl-*N*′-nitro-N-nitrosoguanidine (MNNG) in SH-SY5Y cells assessed 24 h later. Nine pools of compounds were identified that both inhibit PAAN/of MNNG-induced parthanatic cell death. Next, the 90 individual compounds in the 6 pools were synthesized and further assessed for inhibition of PAAN/MIF nuclease activity and MNNG-induced parthanatic cell death. These compounds showed the positive correlation between inhibition of PAAN/MIF nuclease activity and parthanatic cell death (Figure 3D). Among them 12 individual compounds were identified that block PAAN/MIF nuclease activity and MNNG-induced parthanatic cell death by greater than 60% (Figure 3D; Table S1). Dose dependency (0.1–1.0 μM) were assessed for those 12 compounds (C1–C12) against MNNG-induced parthanatic cell death (Figure 3E) and inhibition of PAAN/MIF nuclease activity against the PAAN/MIF substrates (Figure 3F). C7, C8, C11, and C12 were selected for further study because they prominently blocked both MNNG-induced parthanatic cell death and PAAN/MIF nuclease activity.

C7, C8, C11, and C12 did not affect MNNG-induced PARP activation, indicating that they do not have cross-reactivity to PARP inhibition to prevent cell death (Figure S4C). Neither did they inhibit MIF's oxidoreductase activity (Figure S4D) nor its tautomerase activity (Figure S4E). In addition, C7, C8, C11, C12, and the PARP inhibitor ABT-888 did not inhibit staurosporine (STS)-induced apoptotic cell death, while a pan-caspase inhibitor Z-VAD prevented STS-induced cell death (Figure S4F). TNF-α and Z-VAD-induced necroptosis was also not prevented by C7, C8, C11, C12, and ABT-888, while Nec-1 prevented necroptosis (Figure S4G). C7, C8, C11, and C12 did not inhibit the nuclease activity of the structurally related nucleases, *Eco*RI, *Eco*RV, and ExoIII (Figure S4H). Taken together, C7, C8, C11, and C12 selectively prevent parthanatos via inhibiting PAAN/MIF nuclease activity. C7, C8, and C12 attenuated α-syn PFF-induced cell death in mouse cortical neurons, while C11 had no effect (Figure S4I). Both C7 and C11 exhibited basal toxicity without treatment of α-syn PFF when applied to primary cortical neurons (Figure S4I) and thus were not advanced for further study. Both C8 and C12 protected against cell death similar to ABT-888 (Figure 3G) and prevented genomic DNA cleavage (Figure 3H) in human cortical neurons treated with human α-syn PFF. C8 and C12 were further evaluated with regards to their ability to cross the blood-brain barrier (BBB) and only C8 crossed the BBB after oral gavage (Figure 4E).

Identification of PAANIB-1 as a PAAN/MIF nuclease inhibitor

Although C8 can cross the BBB, the achievable concentration (<500 nM) (Figure 4E) is below that required for inhibition of MNNG and α-syn PFF-induced cell death (Figures 3E and 3G). To optimize the potency of C8 and increase its central nervous system (CNS) penetration, we designed and synthesized derivatives of C8 by modifying the tetrapeptide effector domain and the FKBP-binding domain (FKBD), in tandem. The C8 analogs were evaluated for the ability to inhibit PAAN/MIF nuclease activity and cell death and the

ability to cross the BBB (Figure 4A; Table S2). We identified one compound, designated C8-31 (referred to hereafter as parthanatos-associated nuclease inhibitor-1, PAANIB-1) that differs from C8 by the addition of a fluorine (Figure 4B). PAANIB-1 potently inhibited PAAN/MIF nuclease activity and parthanatic cell death (Figure 4A). PAANIB-1 inhibited MNNG-induced parthanatic cell death with an IC_{50} of 0.28 mM and C8 showed an IC_{50} of 0.52 μM (Figure 4C). PAANIB-1, similar to C8, failed to inhibit ABT-888-sensitive PARP activity, STS-induced apoptotic cell, death and TNF-α- and Z-VAD-induced necroptosis (Figures S5A–S5C). Moreover, PAANIB-1 did not enhance tumor viability in PC-3 prostate cancer cells but instead increased tumor toxicity induced by an oxidative DNA-damage-inducing agent, alantolactone (ATL) (Wang et al., 2020), similar to the enhancement of tumor toxicity by the PARP inhibitor, ABT-888 (Figure S5D). Both PAANIB-1 and C8 protected against α-syn PFF-induced cell death in mouse cortical neurons with minor differences in the potency at a lower concentration (Figure 4D). PAANIB-1 pretreatment and 3-day posttreatment after α-syn PFF administration prevented α-syn PFF-induced cell death, while 7- and 10-day posttreatment had no effect (Figure S5E). Levels of PAANIB-1 detected in the brain after oral gavage are almost 3-fold higher than C8 (Figure 4E), underscoring beneficial pharmacokinetic properties endowed from fluorination of C8. PAANIB-1 inhibited PAAN/MIF nuclease activity against its substrates and protected against genomic DNA cleavage in mouse cortical neurons treated with α-syn PFF (Figure 4F), while it did not affect to MIF's or D-DT's cytokine activity (Figure S5F) and nuclease activity of apurinic/apyrimidinic endonuclease (APE1), a human exonuclease that plays a key role in the DNA base excision repair (BER) pathway (Chou and Cheng, 2003) (Figure S5G). Moreover, PAANIB-1 protected against the reduction of the amplitude and frequency of miniature excitatory postsynaptic currents (mEPSCs) and the reduction of nicotinamide adenine dinucleotide (NAD^+) levels induced by α-syn PFF in primary cultured neurons (Figures 4G and S5H; Table S3). Taken together, PAANIB-1 rescues neurons against α-syn-PFF-induced synaptic dysfunction, leading to the reduction in NAD^+ and cell death via inhibition of PAAN/MIF nuclease activity.

Since the rapafucins contain the FKBP-binding domain (Li et al., 2011), rapamycin and FK506 that have the same structural features were evaluated against PAAN/MIF nuclease activity and MNNG-induced parthanatic cell death. Both rapamycin and FK506 failed to inhibit PAAN/MIF nuclease activity (Figure 4H) and MNNG-induced parthanatic cell death (Figure S5I), while PAANIB-1 blocked PAAN/MIF nuclease activity and MNNG-induced parthanatic cell death. On the other hand, PAANIB-1 failed to inhibit rapamycin-sensitive pS6 kinase activity (Figure S5J) and FK506-sensitive calcineurin activity (Figure S5K), indicating no cross-reactivity to other FKBP-related enzymes. To further confirm whether the inhibitory effect of PAANIB-1 on PAAN/MIF's nuclease activity is independent on FKBPs, the role of FKBP12 and 52, the major isoforms of FKBPs (Guo et al., 2019a), were evaluated on the actions of PAANIB-1. Neither FKBP12 or 52 itself has nuclease activity nor do they have an effect on PAANIB-1 inhibition of PAAN/MIF's nuclease activity (Figure S5L). Moreover, depletion of FKBP12 or 52 in SH-SY5Y cells using CRISPR-Cas9 had no effect on MNNG-induced parthanatic cell death and the inhibitory action of PAANIB-1 (Figures S5M and S5N), suggesting that FKBPs are not involved in the cellular mechanism of action of PAANIB-1. MIF tautomerase inhibitors including an

active site inhibitor, ISO-1 (Al-Abed et al., 2005) or allosteric inhibitors, p-425 and Ibudilast (Bai et al., 2012; Cho et al., 2010), failed to inhibit the nuclease activity of PAAN/MIF and parthanatic cell death (Figures 4I and 4J). Taken together, these results indicated that PAANIB-1 is a potent and selective inhibitor for PAAN/MIF nuclease that prevents α-syn PFF-induced cell death. Moreover, PAANIB-1 protection is independent from the FKBP-binding domain and active site and allosteric tautomerase inhibitors of MIF have no effect on PAAN/MIF nuclease activity or parthanatos.

Next, we attempted to gain deeper insight how PAANIB-1 inhibits PAAN/MIF nuclease. PAANIB-1 did not disrupt the interaction of PAAN/MIF with its substrate (Figure S6A). The binding affinity of PAAN/MIF for PAANIB-1 was determined using biolayer interferometry with a K_d value of 1.56 μM (Figure 5A). C8-7, an analog of C8 had no effect on PAAN/MIF nuclease activity and MNNG-induced parthanatic cell death, consistent with its lack of binding to PAAN/MIF (Figures S6B and S6C). A 3D representational model of the PAAN/MIF trimer, an active form of PAAN/MIF nuclease, bound to PAANIB-1, was constructed (Figure S6D). Based on the model, PAAN/MIF amino acids 61–64, 67–68, 73, 98–100, and 106 are potential PAANIB-1-binding sites. Alanine substitutions were made for each residue surrounding the putative binding sites. The nuclease activity of PAAN/MIF S61A, L62A, H63A, S64A (MIF 61–64A), and PAAN/MIF N73A became resistant to PAANIB-1, while that of K67A and I68A (MIF 67–68A) or N98A, Y99A, and Y100A (MIF 98–100A) remained sensitive to inhibition by PAANIB-1 as the WT PAAN/MIF (Figure 5B). PAAN/MIF N106A is devoid of PAAN/MIF nuclease activity (Figure 5B). Individual PAAN/MIF mutants (S61A, L62A, H63A, S64A, K67A, I68A, N73A, N98A, Y99A, Y100A, and N106A) were made and tested against MNNG-induced parthanatic cell death treated with PAANIB-1 in PAAN/MIF KO SH-SY5Y cells in the absence and presence of the latter mutants in comparison with WT, PAAN/MIF 61–64A, PAAN/MIF 67–68A, and PAAN/MIF 98–100A. PAANIB-1 protection against MNNG-induced parthanatic cell death was significantly reduced in the PAAN/MIF L62A, PAAN/MIF 61–64A, and PAAN/MIF N73A mutants (Figures 5C and S6E). The direct binding of the PAAN/MIF WT and alanine mutants was further evaluated against PAANIB-1. PAAN/MIF WT and Y100A mutant exhibited binding to PAANIB-1, while the binding was remarkably decreased for the mutants L62A and N73A (Figure 5D). We also confirmed that PAAN/MIF L62A and N73A failed to show PAANIB-1 protection to α-syn-PFF-induced neuronal death (Figure 5E). PAAN/MIF L62A and N73A did not affect MIF's tautomerase activity (Figure S6F). These results indicate that L62 and N73 residues are involved in the direct binding of PAAN/MIF with PAANIB-1 to inhibit PAAN/MIF nuclease activity.

PAANIB-1 protects PD-related neurodegeneration *in vivo*

The protective role of PAANIB-1 was evaluated by oral administration starting 1 month after the intrastriatal α-syn PFF injection at a time after the pathogenic spread of pathologic α-syn to the substantia nigra and PARP-1 is activated (Kam et al., 2018). Given that 1 μM of PAANIB-1 could prevent 80% of cell death induced by α-syn PFF in primary cortical neurons (Figure 4D), and about 2 μM of PAANIB-1 was found in the brain after oral gavage of 10 mg/kg PAANIB-1 (Figure 4E), we elected to use f a dose of 5 mg/kg for the *in vivo* experiments to mimic the conditions in cell culture and 15 mg/kg to test

whether a higher concentration of PAANIB-1 shows further protective effect (Figure 6A). Mice tolerated the PAANIB-1 with no overt toxicity or weight loss (Figure S7A). WT mice treated with PAANIB-1 exhibited significantly less loss of DA neurons after an intrastriatal injection of α-syn PFF compared with mice treated with vehicle as assessed by stereologic counting of TH immunoreactivity (Figures 6B and 6C) and Nissl staining (Figures 6B and 6D). TH levels were also reduced in WT mice in response to α-syn PFF as determined by western blot analysis, while the reduction in TH levels was prevented in PAANIB-1-treated mice (Figure S7B). α-Syn-PFF-induced reductions in DA (Figure 6E) and its metabolites, DOPAC (Figure 6F) levels, and increase of DA turnover (Figures S7C and S7D) were normalized by both doses of PAANIB-1 treatment. PAANIB-1 also significantly reduced the behavioral deficits elicited by α-syn PFF injection as measured by the pole test (Figures 6G and S7E) and grip strength test (Figures 6H and S7F). Pulse gel electrophoresis indicates that α-syn PFF induced large-scale genomic DNA cleavage in WT mice, while it was significantly attenuated in mice treated with both doses of PAANIB-1 (Figure 6I). Taken together, PAAN/MIF nuclease inhibition by PAANIB-1 protects against α-syn-PFF-induced neurodegeneration in PD.

The effects of PAANIB-1 were further evaluated in an α-synucleinopathy model induced by injection of AAV-human α-syn into substantia nigra (Kirik et al., 2002; Oliveras-Salvá et al., 2013). Treatment with PAANIB-1 in the AAV-human α-syn-injected mice was started 2 weeks after the AAV injection (Figure 7A). Both doses of 5 and 15 mg/kg of PAANIB-1 significantly prevented the α-syn neurodegeneration as assessed by stereologic counting of TH immunoreactivity (Figures 7B and 7C) and Nissl staining (Figures 7B and 7D) and the accompanying behavioral deficits including amphetamine-induced rotation test (Figure 7E), pole test (Figure 7F), and grip strength test (Figure 7G). There is an equivalent expression of α-syn under all conditions (Figures 7H and 7I). We next evaluated whether PAANIB-1 could protect against the loss of DA neurons in the 1-methyl-4-phenyl-1,2,3,6-tetrahydropyridine (MPTP) intoxication model (Mandir et al., 1999; Przedborski et al., 1996). Oral administration of PAANIB-1 protected against the dopaminergic neurodegeneration and behavioral deficits induced by MPTP without affecting the metabolism of MPTP as indicated by the lack of a difference in MPP^+ levels in the different MPTP treatments (Figures 7J–7O).

DISCUSSION

The major findings of this paper are that PAAN/MIF nuclease activity is a druggable target and that pathologic α-syn cell death is mediated through PAAN/MIF nuclease activity. We have demonstrated that genetic depletion of PAAN/MIF prevents pathologic α-syn toxicity both *in vitro* and *in vivo*. Chemical compound screening for PAAN/MIF nuclease inhibitors followed by a secondary screen for inhibitors of parthanatic cell death led to the identification of several inhibitors of PAAN/MIF nuclease activity as well as parthanatic cell death inhibitors. Pharmacological inhibition of PAAN/MIF nuclease prevents neurodegeneration induced by α-syn PFF, AAV-α-syn overexpression or MPTP intoxication *in vivo*.

MIF was previously known to have either tautomerase or nuclease activity (Rosengren et al., 1996; Wang et al., 2016). Use of MIF P2G and PAAN/MIF E22Q knockin mice allowed the separation of the role of PAAN/MIF's nuclease activity from its tautomerase activity in pathologic α-syn neurodegeneration where the nuclease activity was found to be required for neurodegeneration. MIF is also known to act as an atypical extracellular cytokine where it counter regulates the immunosuppressive action of glucocorticoids (Calandra et al., 1995; Flaster et al., 2007; Roger et al., 2005). We showed that there is no significant difference in the ability of PAAN/MIF WT, E22Q, and MIF P2G in blocking the actions of dexamethasone inhibition of LPS-induced TNF-α production suggesting that MIF lacking nuclease activity or tautomerase activity does not interfere with MIF's cytokine function. Recently, MIF was shown to induce the expression of the PD-associated E3 ubiquitin ligase, Parkin, while MIF-deficient murine lungs were shown to have reduced levels of Parkin (Smith et al., 2019). Since Parkin suppresses inflammation through mitochondrial DNA-induced cGAS-STING pathway (Sliter et al., 2018), MIF may play a regulatory role in this process either through its atypical cytokine activity or through its nuclease activity. Future studies will be required to investigate the role of MIF in this pathway.

Similar to glutamate excitotoxicity (Dawson et al., 1991; Eliasson et al., 1997), α-syn PFF increases the formation of nitric oxide and activates PARP-1, which contributes α-syn neurodegeneration by the parthanatic death cascade (Dawson and Dawson, 2017; Kam et al., 2018). Under conditions where PARP-1 activation drives cell death, MIF is the final executioner through its nuclease activity (Wang et al., 2016). Upon PARP-1 activation, PAR leaves the nucleus causing the translocation of mitochondrial AIF (Andrabi et al., 2006; Wang et al., 2011; Yu et al., 2002, 2006) where it recruits PAAN/MIF and translocates to the nucleus leading to PAAN/MIF cleavage of genomic DNA and cell death (Wang et al., 2016; Zhou et al., 2021). Disruption of the AIF-PAAN/MIF interaction or mutation of glutamic acid at position 22 in the catalytic nuclease domain that blocks PAAN/MIF nuclease activity prevents chromatinolysis and cell death (Wang et al., 2016). Mechanistically, α-syn PFF induces an interaction between PAAN/MIF and AIF in a PARP-1-dependent manner, causing the translocation of PAAN/MIF into the nucleus where it acts as a final executioner in parthanatos by cleaving genomic DNA into large-scale fragments, similar to that previously described for glutamate excitotoxicity (Wang et al., 2016). We observed that α-syn PFF increases cleaved genomic DNA both in neuronal culture and *in vivo*, which is suppressed in PAAN/MIF-nuclease-activity-deficient, but not in MIF-tautomerase-activity-deficient mice. These results indicate that interfering with PAAN/MIF's nuclease activity but not MIF tautomerase activity is neuroprotective in pathological α-syn-induced neurodegeneration in PD.

A PAAN/MIF nuclease inhibitor, PAANIB-1 is reported to be bioavailable and brain permeant. Pharmacological inhibition of PAAN/MIF nuclease with PAANIB-1 significantly prevented the loss of DA neurons and rescued the behavioral deficits in the pathologic α-syn PFF model of sporadic PD. PAANIB-1 also protects against the loss of DA neurons and rescued the behavioral deficits in an α-synucleinopathy model induced by injection of AAV-human α-syn into the substantia nigra. The downstream rescue by PAANIB-1 is not due to attenuated α-syn stress since there is an equivalent expression of α-syn under all

conditions. PAANIB-1 also protects against the MPTP intoxication model suggesting that PAANIB-1 may have broad neuroprotective properties.

PAANIB-1 inhibits PAAN/MIF nuclease activity without affecting MIF's tautomerase or cytokine activity. Both active site and allosteric tautomerase inhibitors do not inhibit PAAN/MIF nuclease activity or parthanatos. Thus, MIF nuclease activity is separated from its tautomerase activity. Moreover, PAANIB-1's FKBD does not seem to be involved in the inhibition of PAAN/MIF nuclease activity or parthanatos. Exploration of the mechanism by which PAANIB-1 inhibits PAAN/MIF nuclease activity revealed that PAANIB-1 directly interacts with amino acids L62 and N73 that are distant from the nuclease active site, E22, to inhibit PAAN/MIF nuclease. Future structural studies will need to be conducted to support the biology and the crystal lattice structures of MIF.

PAANIB-1 is highly selective for PAAN/MIF nuclease, which highlights its therapeutic potential. PAANIB-1 clearly shows a specific ability in inhibiting parthanatos since it has no effect on other types of cell death such as apoptosis and necroptosis. Furthermore, it does not affect the upstream activator of parthanatos, PARP-1; thus, it is not likely to affect the physiological function of PARP-1 including DNA-damage repair, gene transcription, or cell proliferation (Bai, 2015; Berger et al., 2018; Fatokun et al., 2014). PAAN/MIF does not share homology with other human DNases and its nuclease activity is separate from its tautomerase activity and cytokine function, making it possible to develop a specific therapeutic target that should have a high safety profile. Since increasing evidence indicates that parthanatos play a prominent role in a wide range of neurologic diseases, including stroke, Parkinson's disease, amyotrophic lateral sclerosis, and Alzheimer's disease (Dawson and Dawson, 2017; McGurk et al., 2019; Park et al., 2020), the therapeutic utility of PAAN/MIF nuclease inhibition will likely extend to other forms of neurodegeneration and cell death where parthanatos plays a role.

Limitations of the study

There are certain limitations of our work that will be the focus of future research. First, while we find that PAAN/MIF nuclease activity is responsible for mediating pathologic α-syn or MPTP-induced loss of DA neurons, we did not molecularly dissect the contributions of cell -autonomous (neuronal) and non-cell-autonomous (glial) mechanisms in the loss of DA neurons in these models. It will be important to investigate whether PAAN/MIF nuclease activity has a regulatory role in other cells of the nervous system including microglia and astrocytes. Second, it will be important to investigate MIF's atypical cytokine activity and innate and adaptive immune regulatory role in the degenerative process of PD. Third, we do not know whether PAANIB-1 is an allosteric or active site inhibitor. Detailed structure activity relationships could enable the identification of more potent next generation small inhibitors of PAAN/MIF nuclease.

STAR★METHODS

RESOURCE AVAILABILITY

Lead contact—Further information and requests for resources should be directed to and will be fulfilled by the lead contact, Ted M. Dawson, M.D., Ph.D. (tdawson@jhmi.edu).

Materials availability—All biological resources, antibodies, cell lines and model organisms and tools are either available through commercial sources or the corresponding authors. The chemical compounds in this paper are currently available via Rapafusyn Inc. Further information and requests for resources and reagents listed in key resources table should be directed to the lead contact.

Data and code availability

- The data sets generated during the current study are available within the paper or from the corresponding author on reasonable request.
- This paper does not report original code.
- Any additional information required to reanalyze the data reported in this paper is available from the lead contact upon request.

EXPERIMENTAL MODEL AND SUBJECT DETAILS

Animals—PAAN/MIF KO (RRID:IMSR_JAX:003830) and MIF P2G KI (RRID:MGI:3842625) mice were obtained from the Jackson Laboratories and backcrossed to C57BL/6 background (RRID:IMSR_JAX:000664). For generation of PAAN/MIF E22Q KI mice, the linearized targeting vector containing the mutated site (E22Q) of PAAN/MIF in exon1 (pDTA-LC-069, AscI) were microinjected into the ES cells and transferred into pseudo-pregnant female mice. Using genomic DNA prepared from tail snip (Proteinase K, Roche Diagnostics; direct PCR lysis, Viagen), pups were genotyped by PCR (GoTag Green Master Mix, Promega) using primers (forward: GGGAGAAATTAATAGTGTGCTCCAG; reverse: CTCAGGGACCTGCTGTGATT G). Positive founders were further confirmed by Sanger sequencing. All housing, breeding, and procedures were performed according to the NIH Guide for the Care and Use of Experimental Animals and approved by Johns Hopkins University Animal Care and Use Committee.

Preparation of human cortical neurons—Human H1 embryonic stem cells (ESCs) were differentiated into cortical neurons as previously described (Xu et al., 2016). Briefly, ESC colonies detached from mouse embryonic fibroblasts (MEFs) were grown in suspension in human ESC medium without FGF2 for 6 days in low-attachment six-well plates (Corning). On day 7, free-floating embryoid bodies (EBs) were transferred to Matrigel coated plates to allow the complete attachment of EB and formation of rosette neuronal aggregates (RONAs). RONAs were manually microisolated and maintained as neurospheres for 1 day and then dissociated into single cells and plated on laminin/poly-D-lysine-coated plates for further experiments. For neuronal differentiation, retinoic acid (2 μM), SHH (50 ng/ml), purmorphamine (2 μM), or the combination of retinoic acid, SHH, and purmorphamine was supplemented in neural differentiation medium containing

Neurobasal/B27 (NB/B27; Invitrogen), brain-derived neurotrophic factor (BDNF; 20 ng/ml; PeproTech), glial cell line–derived neurotrophic factor (GDNF; 20 ng/ml; PeproTech), ascorbic acid (0.2 mM; Sigma), dibutyryl adenosine 3′5′-monophosphate (cAMP; 0.5 mM; Sigma). All experiments using human stem cells were monitored and approved by the JHU Institutional Stem Cell Research Oversight (ISCRO) Committee.

METHOD DETAILS

Preparation of α-syn PFF—Recombinant mouse α-synuclein protein were prepared from IPTG independent inducible pRK172 vector (Luk et al., 2012). Bacterial pellets were resuspended in high-salt buffer [750 mM NaCl, 10 mM Tris (pH 7.6) and 1 mM EDTA] containing a mixture of protease inhibitors (Roche), boiled for 15 min, and centrifuged at 6,000 × g for 20 min. The supernatants were applied onto a Superdex 200 column (GE Healthcare) and Hi-Trap Q HP anion-exchange column (GE Healthcare) and eluted at ~300 mM NaCl. After purification, bacterial endotoxins were eliminated by Toxineraser endotoxin removal kit (GeneScript). α-syn PFF were prepared as previously described (Kam et al., 2018) by agitating (1,000 rpm at 37 °C) for 7 days and sonicated for 30 s (0.5 sec pulse on/off) at 10% amplitude (Branson Digital Sonifier).

Stereotaxic injection of α-syn PFF and AAV-human α-syn—Two to 3-month-old mice were anaesthetized with a mixture of ketamine (100 mg/kg) and xylazine (20 mg/kg) and fixed in a stereotaxic instrument. PBS or α-syn PFF (5 μg/ 2 μl) was unilaterally injected into striatum [anteroposterior (AP) = + 0.2 mm, mediolateral (ML) = + 2.0 mm, dorsoventral (DV) = +2.8 mm from bregma]. AAV-GFP or AAV-human α-syn particles (Vector Biosystems) was unilaterally injected into the SNpc [anteroposterior (AP) = − 3.0 mm, mediolateral (ML) = + 1.2 mm, dorsoventral (DV) = +4.3 mm from bregma]. The infusion was performed at a rate of 0.4 ml/min and the needle were left in place for 5 min for a complete absorption of the solution. After surgery, recovery of animals was monitored the following day of injection. Behavioral tests were performed 6 months after injection and mice were euthanized for biochemical and histological analysis. For biochemical analysis, tissues were immediately dissected and frozen at −80 °C. For histological analysis, animal was perfused with ice-cold PBS followed by 4% paraformaldehyde. Brains were post-fixed with 4% paraformaldehyde and cryoprotected in 30% sucrose.

MPTP treatment—Two to 3-month-old C57BL/6 mice were prepared and PAANIB-1 was administered by oral gavage before, during, and after MPTP administration. The MPTP-treated groups received four intra-peritoneal (i.p.) injections of MPTP•HCl (20 mg/kg free base) in saline at 2 h intervals in a single day (Karuppagounder et al., 2014). Pole test was performed on day 13 and all the mice were sacrificed on day 14.

Behavior Tests—The behavioral deficits in α-syn PFF injected WT, PAAN/MIF KO, E22Q KI or P2G KI mice, in α-syn PFF injected WT or PAAN/MIF KO mice expressing AAV2-Flag-PAAN/MIF WT, E22Q or P2G (ViGene Biosciences), in α-syn PFF injected WT mice delivered with PAANIB-1, in AAV2-human α-syn injected WT mice delivered with PAANIB-1, and in MPTP injected WT mice delivered with PAANIB-1 were assessed by the pole test, grip strength test, clasping test or amphetamine-induced rotation test. The

experimenters were blinded to genotype or treatment condition and randomized. In Figures 1E and 1F, we used 3 males and 4 females for PBS-injected WT, 4 males and 3 females for PBS-injected MIF KO, 3 males and 4 females for α-syn PFF-injected WT, 4 males and 3 females for α-syn PFF-injected MIF KO. In Figures 1J and 1K, we used 3 males and 4 females for PBS-injected WT, 4 males and 3 females for PBS-injected MIF E22Q, 4 males and 4 females for PBS-injected MIF P2G, 4 males and 4 females for α-syn PFF-injected WT, 5 males and 5 females for α-syn PFF-injected MIF E22Q, and 5 males and 5 females for α-syn PFF-injected MIF E22Q. In Figures 6G and 6H, we used 6 males and 7 females for PBS-injected WT with vehicle, 5 males and 5 females for PBS-injected WT with 5 mg/kg PAANIB-1, 7 males and 7 females for PBS-injected WT with 15 mg/kg PAANIB-1, 6 males and 7 females for α-syn PFF-injected WT with vehicle, 10 males and 10 females for α-syn PFF-injected WT with 5 mg/kg PAANIB-1, and 10 males and 10 females for α-syn PFF-injected WT with 15 mg/kg PAANIB-1. In Figures 7E–7G, we used 4 males and 5 females for AAVGFP with vehicle, 5 males and 5 females for AAV-GFP with 15 mg/kg PAANIB-1, 5 males and 6 females for AAV-α-syn with vehicle, 6 males and 5 females for AAV-α-syn with 5 mg/kg PAANIB-1, and 6 males and 5 females for AAV-α-syn with 15 mg/kg PAANIB-1. In Figures 7M and 7N, we used 4 males and 5 females for saline, 5 males and 5 females for saline with 15 mg/kg PAANIB-1, 5 males and 5 females for MPTP, 6 males and 6 females for MPTP with 5 mg/kg PAANIB-1, and 5 males and 5 females for MPTP with 15 mg/kg PAANIB-1.

Pole test: The 9 mm diameter pole is a 2.5 ft metal rod wrapped with bandage gauze. Before the actual test, the mice were trained for two consecutive days and each training session consisted of three test trials. On the day of the test, mice were placed 3 inches from the top of the pole facing head-up. The time to turn and total time to reach the base of the pole were recorded. The maximum cutoff of time to stop the test and recording was 60 s.

Grip strength test: Neuromuscular strength was measured by maximum holding force developed by the mice using a grip-strength meter (Bioseb). Mice were placed onto a metal grid to grasp with either fore or both limbs that are recorded as ‘fore limb’ and ‘fore and hindlimb’, respectively. The tail was gently pulled, and the maximum holding force was recorded by the force transducer before the mice released their grasp on the grid. The peak holding strength was digitally recorded and displayed as force in grams (g).

Clasping test: The hindlimb clasping test is used to show decrease of motor function. The test was performed by grasping the mouse tail and hindlimb clasping was monitored for 10 s (Taylor et al., 2010). Hindlimb clasping was scored as follows: 0, normal (hindlimbs consistently splayed outward, away from the abdomen); 1, one or two hindlimbs partially retracted toward the abdomen for more than 50% of the time; 2, both hindlimbs fully retracted toward the abdomen for more than 50% of the time; 3, hindlimbs pulled into the body and clasped by the forelimbs.

Amphetamine induced stereotypic rotation test: 5 mg/kg amphetamine (Sigma-Aldrich) was intraperitoneally administered to the mice. Mice were placed in a white paper cylinder

of 20 cm diameter and monitored for 60 min. Full body ipsilateral rotations (clockwise) during each ten-minute session were counted for each mouse from the video recordings.

Measurement of dopamine and derivatives: Biogenic amine concentrations were measured by high-performance liquid chromatography with electrochemical detection (HPLC-ECD). Briefly, mice were decapitated, and the striatum was quickly removed from the brain. Striatal tissue was weighed and sonicated in ice-cold 10 μM perchloric acid containing 0.01% EDTA (wt/vol). The 60 ng of 3,4-dihydroxybenzylamine (DHBA) was used as an internal standard. After centrifugation (15,000 × g, 30 min, 4 °C), the supernatant was cleaned through a 0.2 μm filter and 20 μl of the supernatant was injected into HPLC column (3 mm × 150 mm C-18 reverse phase column, AcclaimTM Polar.

Advantage II, Thermo Scientific) and analyzed by a dual channel Coulchem III electrochemical detector (Model 5300, ESA, Inc. Chelmsford, MA). The protein concentrations of tissue homogenates were measured using the BCA protein assay kit (Pierce). Data were normalized to protein concentrations (ng/mg of neurotransmitters/ tissue).

Immunohistochemistry and immunofluorescence—Immunohistochemistry (IHC) and immunofluorescence (IF) were performed on 50 μm thick serial brain sections including substantia nigra and striatum. Every 4th section was utilized for analysis. Primary antibodies (see key resource table) and working dilutions used were as follows: PAAN/MIF (AB_305760), 1:500 (IF); AIF (AB_6266540 1:500 (IF); Flag (AB_439712) 1:1,000 (IHC); TH (AB_10077691) 1:1,000 (IHC, IF); p-α-syn ser129 (AB_2564891) 1:500 (IF). For histological studies, free-floating sections were blocked with 10% goat serum in PBS with 0.2% Triton X-100 and incubated with a 1:1000 dilution of rabbit polyclonal anti-TH (Novus) and visualized with biotinylated goat anti-rabbit IgG, followed by streptavidin-conjugated horseradish peroxidase (HRP) (Vectastain ABC kit, Vector Laboratories). The sections were visualized with SigmaFast DAB peroxidase substrate (Sigma-Aldrich). Sections were counterstained with Nissl (0.09% thionin). Total numbers of TH- and Nissl-stained neurons in the substantia nigra pars compacta were counted by an investigator who was blind to genotypes or treatment condition with randomly allocated group using the optical fractionators, the unbiased method for cell counting by the computer-assisted image analysis system consisting of an Axiophot photomicroscope (Carl Zeiss) equipped with a computer controlled motorized stage (Ludl Electronics), a Hitachi HV C20 camera, and Stereo Investigator software (MicroBright-Field). For Nissl counting, a cell was defined as bright, blue-stained neuronal perikarya with a nucleolus (Karuppagounder et al., 2014). For immunofluorescent studies, double-labeled sections were incubated with a mixture of Alexa-fluor 488- and 594-conjugated secondary antibodies (Invitrogen). The fluorescent images were acquired by confocal scanning microscopy (LSM710, Carl Zeiss). All the images were processed by the Zen software (Carl Zeiss).

Tissue lysate preparation and western blot analysis—Dissected brain regions of interest were homogenized and prepared in lysis buffer [50 mM Tris-HCl (pH 7.4), 150 mM NaCl, 1 mM EDTA, 1% Triton x-100, 0.5% SDS, 0.5% sodium-deoxycholate, phosphatase inhibitor mixture I and II (Sigma-Aldrich), and complete protease inhibitor

mixture (Roche)]. The samples were rotated at 4° C for 30 min for the completed lysis and centrifugated at 15,000 × g for 30 min. Protein concentrations were determined using the BCA assay (Pierce) and samples were separated using SDS polyacrylamide gels and transferred onto nitrocellulose membranes. The blots were blocked with 5% non-fat milk in TBS-T (Tris buffered saline with 0.1% Tween-20) for 1 h, probed using various primary antibodies. Primary antibodies (see key resource table) and working dilutions used were as follows: PAR 1:2,000; PARP-1 (AB_398352), 1:2,000; PAAN/MIF (AB_305760), 1:3,000; AIF (AB_626654) 1:3,000; H3 (AB_105445370), 1:3,000; HSP60 (AB_2295614), 1:1,000; Flag (AB_439712), 1:3,000; pS6K (AB_330944), 1:3,000; S6K (AB_390722), 1:3,000; pS6 (AB_331682), 1:1,000; S6 (AB_331355) 1:3,000; p4E-BP1 (AB_560835), 1:1,000; 4E-BP1 (AB_2097841), 1:3,000; TH (AB_10077691), 1:2,000; DAT (AB_1840807), 1:1,000; FKBP-12 (AB_2102847), 1:1,000; FKBP-52, 1:1,000; p-α-syn ser129 (AB_2564891), 1:1,000; α-syn (AB_398107), 1:1,000; α-syn (Syn 211) (AB_261528), 1:1,000; β-actin_HRP (AB_262011), 1:20,000. Target antigens were incubated with appropriate HRP-conjugated secondary antibodies (Cell signaling) and were visualized by ECL substrate.

Preparation and quantification of genomic DNA—The substantia nigra was rapidly removed from the brain and lysed by repetitive pipetting with a micropipette in lysis buffer [100 mM NaCl, 10 mM Tris-HCl (pH 8.0), 25 mM EDTA (pH 8.0), 0.5 % SDS] with 0.2 mg/ml proteinase K (Roche Diagnostics). Samples were incubated 55° C for overnight and further incubated 85° C for 45 min to inactivate proteinase K. The genomic DNA were immediately separated on a 1.2 % pulse field certified agarose in 0.5 × TBE buffer with initial switch time of 1.5 s and a final switch time of 3.5 s for 12 h at 6 V/cm. The gel was then stained with 0.5 mg/ml Ethidium Bromide (EtBr) and visualized on UV light. Noncleaved genomic DNA was quantified as percentage (%) of the total genomic DNA that included both noncleaved genomic DNA and cleaved genomic DNA in each individual group.

Cell culture, transfection, primary neuronal culture, and treatment—SH-SY5Y cells (ATCC, RRID:CVCL_0019) were cultured in DMEM containing 10% fetal bovine serum and penicillin/streptomycin at 37° C under 5% CO_2. Parthanatos was induced by the treatment of 50 mM MNNG for 15 min in SH-SY5Y cells. ABT-888 or PAAN/MIF inhibitors were pretreated with indicated concentration 1 h before MNNG treatment and cell death was assessed after 24 h. FKBP12 and 52 KO SH-SY5Y cells were generated by CRISPR/Cas9 strategy. The gRNAs targeting FKBP12 (#1, 5’- CAGGTGGAAA CCATCTCCCC-3’; #2, GGTCTGGCCGCGCTTGGGGA-3’) and FKBP52 (#1, 5’-GATGAAGGCGACCGAGAGCG-3’; #2, 5’-CAG CACGCCTTCGTCCTGTT −3’) were ligated to lentiCRISPR vector (Addgene) and transfected into SH-SY5Y cells using PolyFect reagent (Qiagen). Surviving cells after antibiotic selection using puromycin for 3 days were trypsinized and amplified for further analysis. The knockout efficiency was verified by western blot using FKBP12 and 52 antibodies, respectively. Primary cortical neurons from WT, PAAN/MIF KO, E22Q KI, or P2G KI embryos were prepared as previously described (Kam et al., 2016). Briefly, the cortex was dissected and cultured at embryonic day 16 in neurobasal media supplemented with B-27, 0.5 mM L-glutamine, penicillin, and streptomycin (Invitrogen). Primary neurons were infected by lentivirus

carrying PAAN/MIF -WT-Flag, E22Q-Flag, E22A-Flag, P2G-Flag, L62A-Flag or N73A-Flag at days in vitro (DIV) 4–5. ABT-888 or PAAN/MIF inhibitors were applied to neurons 1 h before α-syn PFF treatment. The neuron growth medium was replaced with fresh medium alone or including inhibitors every 3–4 days. α-syn PFF was added at DIV 7 and further incubated for indicated times followed by the cell death assay or biochemical experiments.

Lentivirus, adeno-associated virus (AAV) construction and virus production—Mouse PAAN/MIF-WT-Flag, E22Q-Flag, E22A-Flag, P2G-Flag, L62A-Flag and N73A-Flag were subcloned into a lentiviral cFugw vector (Wang et al., 2016). The lentivirus was produced by transient transfection of the recombinant cFugw vector into 293FT cells together with three packaging vectors: pLP1, pLP2, and pVSV-G (1.3:1.5:1:1.5). The viral supernatants were collected at 48 and 72 hours after transfection and concentrated by ultracentrifugation for 2 hours at 50,000 g. MIF-WT-Flag, MIF E22Q-Flag and MIF-P2G-Flag were subcloned into an AAV-WPRE-bGH vector and produced by the ViGene Biosciences.

Cell death and viability assessment—Primary cultured cortical neurons or human cortical neurons were treated with 5 μg/ml of α-syn PFF for 14 days and cell death was determined by staining of all nuclei with 7 μM Hoechst 33342 and dead cell nuclei with 2 μM propidium iodide (PI) (Invitrogen). The numbers of total and dead cells were counted with the Axiovision 4.6 software (Carl Zeiss). Cell viability was determined by fluorescence at an excitation wavelength 570 nm and an emission wavelength 585 nm using Alamar Blue (Invitrogen).

Immunoprecipitation (IP)—1 mg of whole-cell lysates were incubated with AIF antibody (1 mg/ml, Santa Cruz Biotechnology) overnight, followed by incubation with protein G magnetic beads (Biorad) for 3 h, at 4° C. The IP complexes were washed 5 times and then denatured by boiling for 5 min after adding 2x Laemlli buffer plus b-mercaptoethanol. The samples were analyzed by western blot analysis with mouse anti-Flag antibody (Clone M1, Sigma) or rabbit anti-PAAN/MIF antibody (Abcam).

Subcellular fractionation—Subcellular fraction and quantification of relative levels of AIF and PAAN/MIF were performed as previously described (Wang et al., 2016). Briefly, primary cortical neurons treated with α-syn PFF were subjected to subcellular fractionation into nuclear extracts (N) and postnuclear cell extracts (PN), which is the fraction prepared from whole-cell lysates after removing nuclear proteins using hypotonic buffer (Yu et al., 2002). Each fraction was monitored by H3 antibody (Cell signaling) for the nuclear fraction and HSP60 antibody (Cell signaling) for the postnuclear fraction.

Electrophysiological recordings—Whole-cell patch clamp recordings were obtained from primary cortical neurons visualized under a 40x water immersion objective by fluorescence and DIC optics (Carl Zeiss). Recordings were made with 4–6 MU borosilicate pipettes filled with intracellular solution containing (in mM): K-gluconate 126, KCl 8, HEPES 20, EGTA 0.2, NaCl 2, MgATP 3, Na_3GTP 0.5 (adjust to pH 7.3 with KOH; adjust to 290–300 mOsmol/kg with sucrose). Patchmaster software (HEKA, Lambrecht, Germany)

in combination with an EPC 10 patch-clamp amplifier (HEKA) was used for stimulation and data acquisition. Recordings were made at 32 °C with artificial cerebrospinal fluid (ACSF) containing (in mM): NaCl 125, KCl 2.5, $MgSO_4$ 1, NaH_2PO_4 1.25, $NaHCO_3$ 26, $CaCl_2$ 2, and D-glucose 10. The pH of ACSF was adjusted to 7.4 with NaOH, and osmolarity was at 300–310 mOsmol/kg. Resting membrane potential was recorded in current clamp mode at 0 pA immediately after establishing whole-cell configuration. Series resistance (Rseries) and input resistance (Rin) were calculated from a 5-mV pulse and monitored throughout the experiment. Unstable recordings (>10% fluctuation of Rseries value) during the course of experiments were rejected from further analysis. Recordings were low pass filtered at 2.9 kHz and sampled at 10 kHz. mEPSCs were recorded in voltage-clamp mode with a holding potential of −70 mV, in the presence of TTX (0.25 μM), bicuculline (10 μM), and APV (20 μM), and analyzed using Clampfit 10.5 software (Molecular devices) and MiniAnalysis software (Synaptosoft). 10 cells per condition from three independent cultures were included in the analysis.

PAAN/MIF inhibitor screening strategy—Amine modified PAAN/MIF RF substrate (5'-NH2 -TCCCAAGTAGCTGGGATTACAGGAAAA AAA-3') was immobilized on 96-well DNA-BIND plates (Corning) at a concentration of 100 nM in 100 μl of binding buffer [50 mM Na_2PO_4 (pH 8.5), 1 mM EDTA] at 37° C. After 1 h, the plates were washed three times with PBS to remove the uncoupled substrate and the plates were blocked by adding 200 μl of 3% BSA in binding buffer for 30 min at 37° C. A mixture of 8 μM PAAN/MIF protein and each of 10 μM compound in enzyme reaction buffer [10 mM Tris-Cl (pH 7.0) and 10 mM $MgCl_2$] was added. After 1 h incubation for PAAN/MIF's enzyme reaction, the plates were washed three times with PBS followed by a hybridization reaction adding the biotin labeled complementary DNA (5'-biotin-TTTTTTTCCTGTAA-3') at a 100 nM concentration in 100 μl of hybridization solution (5X SSC and 0.1 % SDS) for 1 h at 55 C. The plates were washed harshly with preheated washing solution (2X SSC and 0.1 % SDS) three times, soaked for 5 min and blocked with 3 % BSA in binding buffer for 30 min. The biotin labeled complementary DNA were incubated with 1:1000 dilution of horseradish peroxidase (HRP)-conjugated Streptavidin (Thermo Scientific) for 30 min at 37 °C and were monitored for colorimetric changes by adding 1-step Ultra TMB-ELISA substrate solution (Thermo Scientific). Each plate contains three reactions with or without PAAN/MIF protein as controls. To assess high-throughput screening (HTS) readiness and robustness of our assay, coefficient of variation (CV), signal-to-background ratio (S/B) and Z' factor were calculated by the value of the reaction without PAAN/MIF and the reaction with PAAN/MIF in each plate. For the secondary screening, SH-SY5Y cells were plated into 96 well plates with 10,000 cells /well. On the next day, each compound was added 1 h before MNNG treatment. Cells were treated with MNNG (50 μM) for 15 min and then further incubated in normal medium including compounds for 24 h. Cell viability was determined using Alamar Blue as described above.

Nuclease assay—Purified PAAN/MIF protein (4 μM) was incubated with compounds (10 μM) in the nuclease buffer [10 mM Tris-Cl (pH 7.0) and 10 mM $MgCl_2$] for 20 min on ice. Then samples were added with 1 μM of PAAN/MIF substrate and incubated for 1 h at 37° C. The reaction was terminated with loading buffer containing 10 mM EDTA and separated

on 15 % TBE-urea polyacrylamide (PAGE) gel or 20 % TBE PAGE gel. For other nucleases (EcoRI and EcoRV) assays, pcDNA3 (500 ng/reaction) was used as a substrate and 0.01 unit of Exonulcase III were incubated with small dsDNA (5'-GTCACCGTCATACGACTC-3' and 5'-GAGTCGTATGACGGTGAC-3'). For APE1 endonuclease assays, 40-mer of dsDNA (5'-GTGGCGCGGAGACTTAGAGAFATTTGGCGCGGGGAATTCC-3' and 5'-CACCGC GCCTCTGAA TCTCTGTAAACCGCGCCCCTTAAGG-3') used as a substrate (Chou and Cheng, 2003).

Purification of PAAN/MIF recombinant proteins—Human PAAN/MIF (NM_002415) cDNA and its variants were subcloned into pGEX-6P-1 vector (GE Healthcare) and mutants were generated using a QuikChange site-directed mutagenesis kit (Agilent Technologies). The sequences were confirmed by automated DNA sequencing. The protein was expressed and purified from Escherichia coli by glutathione sepharose (GE Healthcare). The GST tag was subsequently proteolytically removed. GST protein was used as a negative control in the nuclease assay and PAAN/MIF proteins purified by FPLC using Superdex 200 10/300GL column (GE Healthcare, Life Sciences) were also used in the nuclease assays.

Biolayer interferometry assay—The dose-dependent binding of PAANIB-1 for PAAN/MIF WT or PAAN/MIF variants were determined by a biolayer interferometry assay using Octet RED96 (ForteBio) (Wang et al., 2019). All the proteins used in this assay were tagged with GST. Anti-GST biosensor tips (ForteBio) were used to immobilize the GST proteins after prewetting with 1X kinetic buffer (ForteBio). The equilibrated GST biosensors were loaded with PAAN/MIF WT or variants (25 μg/ml). Background binding controls were measured by sensors that were incubated in buffer without proteins. All assays were performed by a standard protocol in 96-well black plates (Greiner Bio) with a total volume of 200 μl per well. All the data were analyzed by Octet data analysis software.

In vitro ribosylation assay of PARP-1—1 mg of recombinant PARP-1 activated DNA and NAD^+ (Trevigen) in the presence or absence of 1 μM of PARP-1 inhibitor, ABT-888 or PAAN/MIF inhibitors (C8 or PAANIB-1) were incubated in the PARP assay buffer (Trevigen) for 30 min at room temperature and analyzed by immunoblot analysis using PAR antibody.

Calcineurin activity assay—Calcineurin activity was measured using a calcineurin cellular activity assay (Enzo Life Sciences) according to manufacturer's protocols (Sangadala et al., 2019). SH-SY5Y cells treated with FK506, or PAANIB-1 were placed in a desalting column to remove excess phosphates and nucleotides. Total phosphate activity was determined in the samples by incubating with a calcineurin-specific substrate supplied in the manufacturer and measured by monitoring absorbance at 620 nm. Calcineurin activity was calculated as the difference between total phosphatase activity minus the phosphatase activity in the presence of 10 mM EGTA that blocks calcineurin activity.

Electrophoretic mobility shift assay (EMSA)—EMSA assays were performed using the Light-Shift Chemiluminescent EMSA kit (Thermo Scientific) following the manufactures instruction. Recombinant PAAN/MIF protein (2 μM) was incubated with 1–100 μM PAANIB-1 as indicated in the binding buffer containing 10 mM $MgCl_2$ for 10

min and further incubated with biotin-labeled DNA substrates (10 nM) for 30 min on ice. The mixture was separated on 6 % retardation polyacrylamide and transferred to a Nylon membrane. Immunoblot analysis was performed to detect the biotin-labeled DNA using the Chemiluminescent Nucleic Acid Detection Module (Thermo Scientific).

NAD assay—NAD^+ were measured according to the manufacturer's instructions of the assay kit (Abcam). Briefly, α-syn PFF treated primary cortical neurons with or without PAANIB-1 were lysed in NAD extraction buffer and the protein concentration was determined (BioRad Laboratories). The same amount of protein was used for each sample. Samples were divided, half was used to heat degrade NAD^+, and the other half represents total NAD. Samples were then mixed with reaction buffer and Cycling Enzyme to transform all NAD^+ in NADH, allowing the measure of total NAD (NADt). Concentration of NAD^+ and NADH was then calculated by comparison to NADH standard curve.

Oxidoreductase activity assay—The thiol-protein oxidoreductase activity of PAAN/MIF was measured using insulin as the substrate as described previously (Kudrin et al., 2006). Briefly, the insulin assay is based on the reduction of insulin and subsequent insolubilization of the insulin β-chain. The time-dependent increase in turbidity is then measured spectrophotometrically at 650 nm. The reaction was started by adding 5 μM PAAN/MIF WT in the presence or absence of 10 μM compounds (C7, C8, C11 and C12) dissolved in 20 mM sodium phosphate buffer (pH 7.2), and 200 mM reduced glutathione (GSH) to ice-cold reaction mixture containing 1 mg/ml insulin, 100 mM sodium phosphate buffer (pH 7.2) and 2 mM EDTA. Insulin reduction was measured against the control solution (containing GSH) in the same experiment.

Tautomerase activity assay—The keto-enol tautomeric conversion of D-dopachrome methyl ester by PAAN/MIF was used as described previously (Bendrat et al., 1997). Briefly, a fresh solution of D-dopachrome methyl ester was prepared by mixing 2 mM L-3,4 dihydroxyphenylalanine methyl ester with 4 mM sodium peroxidate for 5 min at room temperature and then placed directly on ice before use. The enzymatic reaction was initiated at 25° C by adding 20 μl of the dopachrome methyl ester substrate to 200 μl of PAAN/MIF WT (final concentration 5 μM) with or without 10 μM compounds (C7, C8, C11 and C12) in tautomerase assay buffer (50 mM potassium phosphate, 1mM EDTA, pH 6.0). To enhance substrate stability, excess sodium meta-periodate was removed using C8 disposable columns (Waters). The activity was determined by the decrease in absorbance at 475 nm using a spectrophotometer (Molecular Devices).

Glucocorticoid overriding assay—Primary microglia cells were pre-incubated for 1 h with 100 nM dexamethasone (Sigma) and MIF or D-DT with or without PAANIB-1 before adding 100 ng/ml LPS (Sigma). TNFα levels were measured by comparative quantitative real time PCR (qPCR) (Merk et al., 2011). Total RNA was extracted with RNA isolation kit (Qiagen) and then reverse-transcribed to cDNA using the High-Capacity cDNA Reverse Transcription System (Life Technologies). qPCR was performed in duplicated or triplicated for each sample using fast SYBR Green Master Mix (Life Technologies) and ViiA 7 Real-

Time PCR System (Applied Biosystems). The expression levels of TNFα were normalized to the expression of β-actin.

Preparation of PAANIB-1—Rapafucins, including C8 and PAANIB-1 and other analogues were synthesized using solid-phase peptide synthesis and catalytic ring-closing metathesis and purified on a silica gel column. FKBD and cis-C6 linker conjugated resin was prepared as previously described[22]. Modified FKBDs, including eFKBD-E1A24168 were prepared by BioDuro. PAANIB-1 used for in vivo studies was further purified using reverse-phase column chromatography to remove any metal catalyst residues. HPLC-MS was used to analyze purity and identification for all compounds synthesized. HRMS was measured for key compounds for further verification. HRMS for C8 [M+H] + C62H83N6O15, calculated: 1151.5916, observed: 1151.5900, HRMS for PAANIB-1 [M+H]+ C62H82FN6O15, calculated: 1169.5822, observed: 1169.5802. PAANIB-1 or other PAAN/MIF inhibitors were dissolved in dimethyl sulfoxide (DMSO) (Sigma-Al-drich) for in vitro assays. PAANIB-1 was dissolved in a vehicle solution of 1 % Tween 80 (Sigma-Aldrich), 10% polyethylene glycol (PEG 400, Fluka) and 1 % hydroxy propyl methyl cellulose (HPMC, Sigma-Aldrich) for oral administration.

Measurement of PAANIB-1 in brain—C8, C12 and PAANIB-1 were resuspended in a vehicle solution and were administered at 10 mg/kg by oral gavage. After 2 h, mice were perfused with PBS and whole brain was isolated, weighed and grounded with a pestle to a very fine powder with liquid nitrogen. Then, 2-folds of acetonitrile were added to brain tissue sample and the mixture was centrifuged at 14,000 rpm, 4° C for 10 min. The supernatant was used for analysis. The concentration of compounds in brain tissue were measured using HPLC-MS on a C-18 reverse phase HPLC column. Separations were achieved using a linear gradient of buffer B from 40% to 95% in A (A = 0.1% formic acid in H_2O; B = 0.1% formic acid in CH_3CN) at a flow rate of 1 ml/min. Intracerebroventricular (ICV) injected brain samples at 0.5, 1, 2, 4 or 8 μM concentration were used for the standard curve.

QUANTIFICATION AND STATISTICAL ANALYSIS

All data are represented as mean ± s.e.m. with at least 3 independent experiments. Statistical analysis was performed using GraphPad Prism 7 and statistical significance were reported in the relevant Figures and Figure legends. Differences between 2 means and among multiple means were assessed by unpaired two-tailed student t test and ANOVA followed by Tukey's post hoc test, respectively. The graph representation, definition of n and which statistical test was performed is indicated in the figure legend. Error bars show standard error of the mean (SEM) or standard deviation (SD), as indicated in the figure legend. Sample size was chosen according to that used for similar experiments in the literature.

Supplementary Material

Refer to Web version on PubMed Central for supplementary material.

ACKNOWLEDGMENTS

This work was supported by grants from the NIH R37 NS067525, the JPB Foundation, the Farmer Family Foundation and in part through a sponsored research agreement with Neuraly. T.M.D. is the Leonard and Madlyn Abramson Professor in neurodegenerative diseases. The authors acknowledge the joint participation by the Adrienne Helis Malvin Medical Research Foundation through its direct engagement in the continuous active conduct of medical research in conjunction with the Johns Hopkins Hospital and the Johns Hopkins University School of Medicine and the Foundation's Parkinson's Disease Program M-2016. The rapafucin-related work was also supported by FAMRI and a generous gift from Mr. Shengjun Yan and Ms. Hongju Mao as well as a sponsored research support from Rapafusyn Pharmaceuticals. The PAANIB-1 for the *in vivo* study was kindly provided by Rapafusyn Pharmaceuticals.

REFERENCES

Al-Abed Y, Dabideen D, Aljabari B, Valster A, Messmer D, Ochani M, Tanovic M, Ochani K, Bacher M, Nicoletti F, et al. (2005). ISO-1 binding to the tautomerase active site of MIF inhibits its pro-inflammatory activity and increases survival in severe sepsis. J. Biol. Chem 280, 36541–36544. 10.1074/jbc.C500243200. [PubMed: 16115897]

Andrabi SA, Kim NS, Yu SW, Wang H, Koh DW, Sasaki M, Klaus JA, Otsuka T, Zhang Z, Koehler RC, et al. (2006). Poly(ADP-ribose) (PAR) polymer is a death signal. Proc. Natl. Acad. Sci. USA 103, 18308–18313. 10.1073/pnas.0606526103. [PubMed: 17116882]

Bai F, Asojo OA, Cirillo P, Ciustea M, Ledizet M, Aristoff PA, Leng L, Koski RA, Powell TJ, Bucala R, and Anthony KG (2012). A novel allosteric inhibitor of macrophage migration inhibitory factor (MIF). J. Biol. Chem 287, 30653–30663. 10.1074/jbc.M112.385583. [PubMed: 22782901]

Bai P (2015). Biology of poly(ADP-ribose) polymerases: the factotums of cell maintenance. Mol. Cell 58, 947–958. 10.1016/j.molcel.2015.01.034. [PubMed: 26091343]

Bendrat K, Al-Abed Y, Callaway DJ, Peng T, Calandra T, Metz CN, and Bucala R (1997). Biochemical and mutational investigations of the enzymatic activity of macrophage migration inhibitory factor. Biochemistry 36, 15356–15362. 10.1021/bi971153a. [PubMed: 9398265]

Berger NA, Besson VC, Boulares AH, Bürkle A, Chiarugi A, Clark RS, Curtin NJ, Cuzzocrea S, Dawson TM, Dawson VL, et al. (2018). Opportunities for the repurposing of PARP inhibitors for the therapy of non-oncological diseases. Br. J. Pharmacol 175, 192–222. 10.1111/bph.13748. [PubMed: 28213892]

Bloom J, Sun S, and Al-Abed Y (2016). MIF, a controversial cytokine: a review of structural features, challenges, and opportunities for drug development. Expert Opin. Ther. Targets 20, 1463–1475. 10.1080/14728222.2016.1251582. [PubMed: 27762152]

Bozza M, Satoskar AR, Lin G, Lu B, Humbles AA, Gerard C, and David JR (1999). Targeted disruption of migration inhibitory factor gene reveals its critical role in sepsis. J. Exp. Med 189, 341–346. 10.1084/jem.189.2.341. [PubMed: 9892616]

Bucala R (1996). MIF rediscovered: cytokine, pituitary hormone, and glucocorticoid-induced regulator of the immune response. FASEB J 10, 1607–1613. 10.1096/fasebj.10.14.9002552. [PubMed: 9002552]

Calandra T, Bernhagen J, Metz CN, Spiegel LA, Bacher M, Donnelly T, Cerami A, and Bucala R (1995). MIF as a glucocorticoid-induced modulator of cytokine production. Nature 377, 68–71. 10.1038/377068a0. [PubMed: 7659164]

Cho Y, Crichlow GV, Vermeire JJ, Leng L, Du X, Hodsdon ME, Bucala R, Cappello M, Gross M, Gaeta F, et al. (2010). Allosteric inhibition of macrophage migration inhibitory factor revealed by ibudilast. Proc. Natl. Acad. Sci. USA 107, 11313–11318. 10.1073/pnas.1002716107. [PubMed: 20534506]

Chou KM, and Cheng YC (2003). The exonuclease activity of human apurinic/apyrimidinic endonuclease (APE1). Biochemical properties and inhibition by the natural dinucleotide Gp4G. J. Biol. Chem 278, 18289–18296. 10.1074/jbc.M212143200. [PubMed: 12624104]

Dawson TM, and Dawson VL (2017). Mitochondrial mechanisms of neuronal cell death: potential therapeutics. Annu. Rev. Pharmacol. Toxicol 57, 437–454. 10.1146/annurev-pharmtox-010716-105001. [PubMed: 28061689]

Dawson VL, Dawson TM, London ED, Bredt DS, and Snyder SH (1991). Nitric oxide mediates glutamate neurotoxicity in primary cortical cultures. Proc. Natl. Acad. Sci. USA 88, 6368–6371. 10.1073/pnas.88.14.6368. [PubMed: 1648740]

Eliasson MJ, Sampei K, Mandir AS, Hurn PD, Traystman RJ, Bao J, Pieper A, Wang ZQ, Dawson TM, Snyder SH, and Dawson VL (1997). Poly(ADP-ribose) polymerase gene disruption renders mice resistant to cerebral ischemia. Nat. Med 3, 1089–1095. 10.1038/nm1097-1089. [PubMed: 9334719]

Fatokun AA, Dawson VL, and Dawson TM (2014). Parthanatos: mitochondrial-linked mechanisms and therapeutic opportunities. Br. J. Pharmacol 171, 2000–2016. 10.1111/bph.12416. [PubMed: 24684389]

Fingerle-Rowson G, Kaleswarapu DR, Schlander C, Kabgani N, Brocks T, Reinart N, Busch R, Schütz A, Lue H, Du X, et al. (2009). A tautomerase-null macrophage migration-inhibitory factor (MIF) gene knock-in mouse model reveals that protein interactions and not enzymatic activity mediate MIF-dependent growth regulation. Mol. Cell. Biol 29, 1922–1932. 10.1128/MCB.01907-08. [PubMed: 19188446]

Flaster H, Bernhagen J, Calandra T, and Bucala R (2007). The macrophage migration inhibitory factor-glucocorticoid dyad: regulation of inflammation and immunity. Mol. Endocrinol 21, 1267–1280. 10.1210/me.2007-0065. [PubMed: 17389748]

Fujiwara H, Hasegawa M, Dohmae N, Kawashima A, Masliah E, Goldberg MS, Shen J, Takio K, and Iwatsubo T (2002). α-Synuclein is phosphorylated in synucleinopathy lesions. Nat. Cell Biol 4, 160–164. 10.1038/ncb748. [PubMed: 11813001]

Guo Z, Cheng Z, Wang J, Liu W, Peng H, Wang Y, Rao AVS, Li RJ, Ying X, Korangath P, et al. (2019a). Discovery of a potent GLUT inhibitor from a library of Rapafucins by using 3D microarrays. Angew. Chem. Int. Ed. Engl 58, 17158–17162. 10.1002/anie.201905578. [PubMed: 31591797]

Guo Z, Hong SY, Wang J, Rehan S, Liu W, Peng H, Das M, Li W, Bhat S, Peiffer B, et al. (2019b). Rapamycin-inspired macrocycles with new target specificity. Nat. Chem 11, 254–263. 10.1038/s41557-018-0187-4. [PubMed: 30532015]

Henderson MX, Trojanowski JQ, and Lee VM (2019). α-Synuclein pathology in Parkinson's disease and related α-synucleinopathies. Neurosci. Lett 709, 134316. 10.1016/j.neulet.2019.134316. [PubMed: 31170426]

Hermanowski-Vosatka A, Mundt SS, Ayala JM, Goyal S, Hanlon WA, Czerwinski RM, Wright SD, and Whitman CP (1999). Enzymatically inactive macrophage migration inhibitory factor inhibits monocyte chemotaxis and random migration. Biochemistry 38, 12841–12849. 10.1021/bi991352p. [PubMed: 10504254]

Kam TI, Mao X, Park H, Chou SC, Karuppagounder SS, Umanah GE, Yun SP, Brahmachari S, Panicker N, Chen R, et al. (2018). Poly(ADP-ribose) drives pathologic α-synuclein neurodegeneration in Parkinson's disease. Science 362. 10.1126/science.aat8407.

Kam TI, Park H, Gwon Y, Song S, Kim SH, Moon SW, Jo DG, and Jung YK (2016). FcγRIIb-SHIP2 axis links Aβ to tau pathology by disrupting phosphoinositide metabolism in Alzheimer's disease model. eLife 5, e18691. 10.7554/eLife.18691. [PubMed: 27834631]

Karuppagounder SS, Brahmachari S, Lee Y, Dawson VL, Dawson TM, and Ko HS (2014). The c-Abl inhibitor, nilotinib, protects dopaminergic neurons in a preclinical animal model of Parkinson's disease. Sci. Rep 4, 4874. 10.1038/srep04874. [PubMed: 24786396]

Kirik D, Rosenblad C, Burger C, Lundberg C, Johansen TE, Muzyczka N, Mandel RJ, and BjÖrklund A (2002). Parkinson-like neurodegeneration induced by targeted overexpression of α-synuclein in the nigrostriatal system. J. Neurosci 22, 2780–2791. . [PubMed: 11923443]

Kudrin A, Scott M, Martin S, Chung CW, Donn R, McMaster A, Ellison S, Ray D, Ray K, and Binks M (2006). Human macrophage migration inhibitory factor: a proven immunomodulatory cytokine? J. Biol. Chem 281, 29641–29651. 10.1074/jbc.M601103200. [PubMed: 16893895]

Lengyel-Zhand Z, Puentes LN, and Mach RH (2022). PARkinson's: From cellular mechanisms to potential therapeutics. Pharmacol. Ther 230, 107968. 10.1016/j.pharmthera.2021.107968. [PubMed: 34391789]

Li W, Bhat S, and Liu JO (2011). A simple and efficient route to the FKBP-binding domain from rapamycin. Tetrahedron Lett. 52, 5070–5072. 10.1016/j.tetlet.2011.07.094. [PubMed: 21894238]

Lord CJ, and Ashworth A (2017). PARP inhibitors: synthetic lethality in the clinic. Science 355, 1152–1158. 10.1126/science.aam7344. [PubMed: 28302823]

Luk KC, Kehm V, Carroll J, Zhang B, O'Brien P, Trojanowski JQ, and Lee VM (2012). Pathological α-synuclein transmission initiates Parkinson-like neurodegeneration in nontransgenic mice. Science 338, 949–953. 10.1126/science.1227157. [PubMed: 23161999]

Mandir AS, Przedborski S, Jackson-Lewis V, Wang ZQ, SimbulanRosenthal CM, Smulson ME, Hoffman BE, Guastella DB, Dawson VL, and Dawson TM (1999). Poly(ADP-ribose) polymerase activation mediates 1-methyl-4-phenyl-1, 2,3,6-tetrahydropyridine (MPTP)-induced parkinsonism. Proc. Natl. Acad. Sci. USA 96, 5774–5779. 10.1073/pnas.96.10.5774. [PubMed: 10318960]

Mao X, Ou MT, Karuppagounder SS, Kam TI, Yin X, Xiong Y, Ge P, Umanah GE, Brahmachari S, Shin JH, et al. (2016). Pathological α-synuclein transmission initiated by binding lymphocyte-activation gene 3. Science 353, aah3374. 10.1126/science.aah3374. [PubMed: 27708076]

McGurk L, Rifai OM, and Bonini NM (2019). Poly(ADP-ribosylation) in agerelated neurological disease. Trends Genet. 35, 601–613. 10.1016/j.tig.2019.05.004. [PubMed: 31182245]

Merk M, Zierow S, Leng L, Das R, Du X, Schulte W, Fan J, Lue H, Chen Y, Xiong H, et al. (2011). The D-dopachrome tautomerase (DDT) gene product is a cytokine and functional homolog of macrophage migration inhibitory factor (MIF). Proc. Natl. Acad. Sci. USA 108, E577–E585. 10.1073/pnas.1102941108. [PubMed: 21817065]

Metz CN, and Bucala R (1997). Role of macrophage migration inhibitory factor in the regulation of the immune response. Adv. Immunol 66, 197–223. 10.1016/s0065-2776(08)60598-2. [PubMed: 9328642]

Oliveras-Salvá M, Van der Perren A, Casadei N, Stroobants S, Nuber S, D'Hooge R, Van den Haute C, and Baekelandt V (2013). rAAV2/7 vector-mediated overexpression of α-synuclein in mouse substantia nigra induces protein aggregation and progressive dose-dependent neurodegeneration. Mol. Neurodegener 8, 44. 10.1186/1750-1326-8-44. [PubMed: 24267638]

Paralkar V, and Wistow G (1994). Cloning the human gene for macrophage migration inhibitory factor (MIF). Genomics 19, 48–51. 10.1006/geno.1994.1011. [PubMed: 8188240]

Park H, Kam TI, Dawson TM, and Dawson VL (2020). Poly (ADP-ribose) (PAR)-dependent cell death in neurodegenerative diseases. Int. Rev. Cell Mol. Biol 353, 1–29. 10.1016/bs.ircmb.2019.12.009.

Przedborski S, Jackson-Lewis V, Yokoyama R, Shibata T, Dawson VL, and Dawson TM (1996). Role of neuronal nitric oxide in 1-methyl-4-phenyl-1,2,3,6-tetrahydropyridine (MPTP)-induced dopaminergic neurotoxicity. Proc. Natl. Acad. Sci. USA 93, 4565–4571. 10.1073/pnas.93.10.4565. [PubMed: 8643444]

Puentes LN, Lengyel-Zhand Z, Lee JY, Hsieh CJ, Schneider ME Jr., Edwards KJ, Luk KC, Lee VM, Trojanowski JQ, and Mach RH (2021). Poly (ADP-ribose) interacts with phosphorylated α-synuclein in post mortem PD samples. Front. Aging Neurosci 13, 704041. 10.3389/fnagi.2021.704041. [PubMed: 34220490]

Roger T, Chanson AL, Knaup-Reymond M, and Calandra T (2005). Macrophage migration inhibitory factor promotes innate immune responses by suppressing glucocorticoid-induced expression of mitogen-activated protein kinase phosphatase-1. Eur. J. Immunol 35, 3405–3413. 10.1002/eji.200535413. [PubMed: 16224818]

Rosengren E, Bucala R, Aman P, Jacobsson L, Odh G, Metz CN, and Rorsman H (1996). The immunoregulatory mediator macrophage migration inhibitory factor (MIF) catalyzes a tautomerization reaction. Mol. Med 2, 143–149. [PubMed: 8900542]

Sangadala S, Devereaux EJ, Presciutti SM, Boden SD, and Willet NJ (2019). FK506 induces ligand-independent activation of the bone morphogenetic protein pathway and osteogenesis. Int. J. Mol. Sci 20, 1900. 10.3390/ijms20081900.

Sliter DA, Martinez J, Hao L, Chen X, Sun N, Fischer TD, Burman JL, Li Y, Zhang Z, Narendra DP, et al. (2018). Parkin and PINK1 mitigate STING-induced inflammation. Nature 561, 258–262. 10.1038/s41586-018-0448-9. [PubMed: 30135585]

Smith CA, Tyrell DJ, Kulkarni UA, Wood S, Leng L, Zemans RL, Bucala R, and Goldstein DR (2019). Macrophage migration inhibitory factor enhances influenza-associated mortality in mice. JCI Insight 4, e128034. 10.1172/jci.insight.128034.

Taylor TN, Greene JG, and Miller GW (2010). Behavioral phenotyping of mouse models of Parkinson's disease. Behav. Brain Res 211, 1–10. 10.1016/j.bbr.2010.03.004. [PubMed: 20211655]

Ueda J, Uemura N, Sawamura M, Taguchi T, Ikuno M, Kaji S, Taruno Y, Matsuzawa S, Yamakado H, and Takahashi R (2021). Perampanel inhibits α-synuclein transmission in Parkinson's disease models. Mov. Disord 36, 1554–1564. 10.1002/mds.28558. [PubMed: 33813737]

Wang H, Zhang S, Song L, Qu M, and Zou Z (2020). Synergistic lethality between PARP-trapping and alantolactone-induced oxidative DNA damage in homologous recombination-proficient cancer cells. Oncogene 39, 2905–2920. 10.1038/s41388-020-1191-x. [PubMed: 32029902]

Wang L, Zhang L, Li L, Jiang J, Zheng Z, Shang J, Wang C, Chen W, Bao Q, Xu X, et al. (2019). Small-molecule inhibitor targeting the Hsp90-Cdc37 protein-protein interaction in colorectal cancer. Sci. Adv 5, eaax2277. 10.1126/sciadv.aax2277. [PubMed: 31555737]

Wang X, and Ge P (2020). Parthanatos in the pathogenesis of nervous system diseases. Neuroscience 449, 241–250. 10.1016/j.neuroscience.2020.09.049. [PubMed: 33039521]

Wang Y, An R, Umanah GK, Park H, Nambiar K, Eacker SM, Kim B, Bao L, Harraz MM, Chang C, et al. (2016). A nuclease that mediates cell death induced by DNA damage and poly(ADP-ribose) polymerase-1. Science 354. 10.1126/science.aad6872.

Wang Y, Kim NS, Haince JF, Kang HC, David KK, Andrabi SA, Poirier GG, Dawson VL, and Dawson TM (2011). Poly(ADP-ribose) (PAR) binding to apoptosis-inducing factor is critical for PAR polymerase-1-dependent cell death (parthanatos). Sci. Signal 4, ra20. 10.1126/scisignal.2000902. [PubMed: 21467298]

Xu JC, Fan J, Wang X, Eacker SM, Kam TI, Chen L, Yin X, Zhu J, Chi Z, Jiang H, et al. (2016). Cultured networks of excitatory projection neurons and inhibitory interneurons for studying human cortical neurotoxicity. Sci. Transl. Med 8, 333ra48. 10.1126/scitranslmed.aad0623.

Yamada K, and Iwatsubo T (2018). Extracellular α-synuclein levels are regulated by neuronal activity. Mol. Neurodegener 13, 9. 10.1186/s13024-018-0241-0. [PubMed: 29467003]

Yang D, Shu T, Zhao H, Sun Y, Xu W, and Tu G (2020). Knockdown of macrophage migration inhibitory factor (MIF), a novel target to protect neurons from parthanatos induced by simulated post-spinal cord injury oxidative stress. Biochem. Biophys. Res. Commun 523, 719–725. 10.1016/j.bbrc.2019.12.115. [PubMed: 31948762]

Yu SW, Andrabi SA, Wang H, Kim NS, Poirier GG, Dawson TM, and Dawson VL (2006). Apoptosis-inducing factor mediates poly(ADP-ribose) (PAR) polymer-induced cell death. Proc. Natl. Acad. Sci. USA 103, 18314–18319. 10.1073/pnas.0606528103. [PubMed: 17116881]

Yu SW, Wang H, Poitras MF, Coombs C, Bowers WJ, Federoff HJ, Poirier GG, Dawson TM, and Dawson VL (2002). Mediation of poly(ADP-ribose) polymerase-1-dependent cell death by apoptosis-inducing factor. Science 297, 259–263. 10.1126/science.1072221. [PubMed: 12114629]

Zandarashvili L, Langelier MF, Velagapudi UK, Hancock MA, Steffen JD, Billur R, Hannan ZM, Wicks AJ, Krastev DB, Pettitt SJ, et al. (2020). Structural basis for allosteric PARP-1 retention on DNA breaks. Science 368, eaax6367. 10.1126/science.aax6367. [PubMed: 32241924]

Zhou Y, Liu L, Tao S, Yao Y, Wang Y, Wei Q, Shao A, and Deng Y (2021). Parthanatos and its associated components: promising therapeutic targets for cancer. Pharmacol. Res 163, 105299. 10.1016/j.phrs.2020.105299. [PubMed: 33171306]

Highlights

- Pathologic α-synuclein neurodegeneration occurs via PAAN/MIF nuclease activity
- Genetic depletion and nuclease-deficient MIF prevents α-synuclein neurodegeneration
- Identification of a first-in class MIF nuclease inhibitor, PAANIB-1
- PAANIB-1 prevents neurodegeneration in multiple models of Parkinson's disease

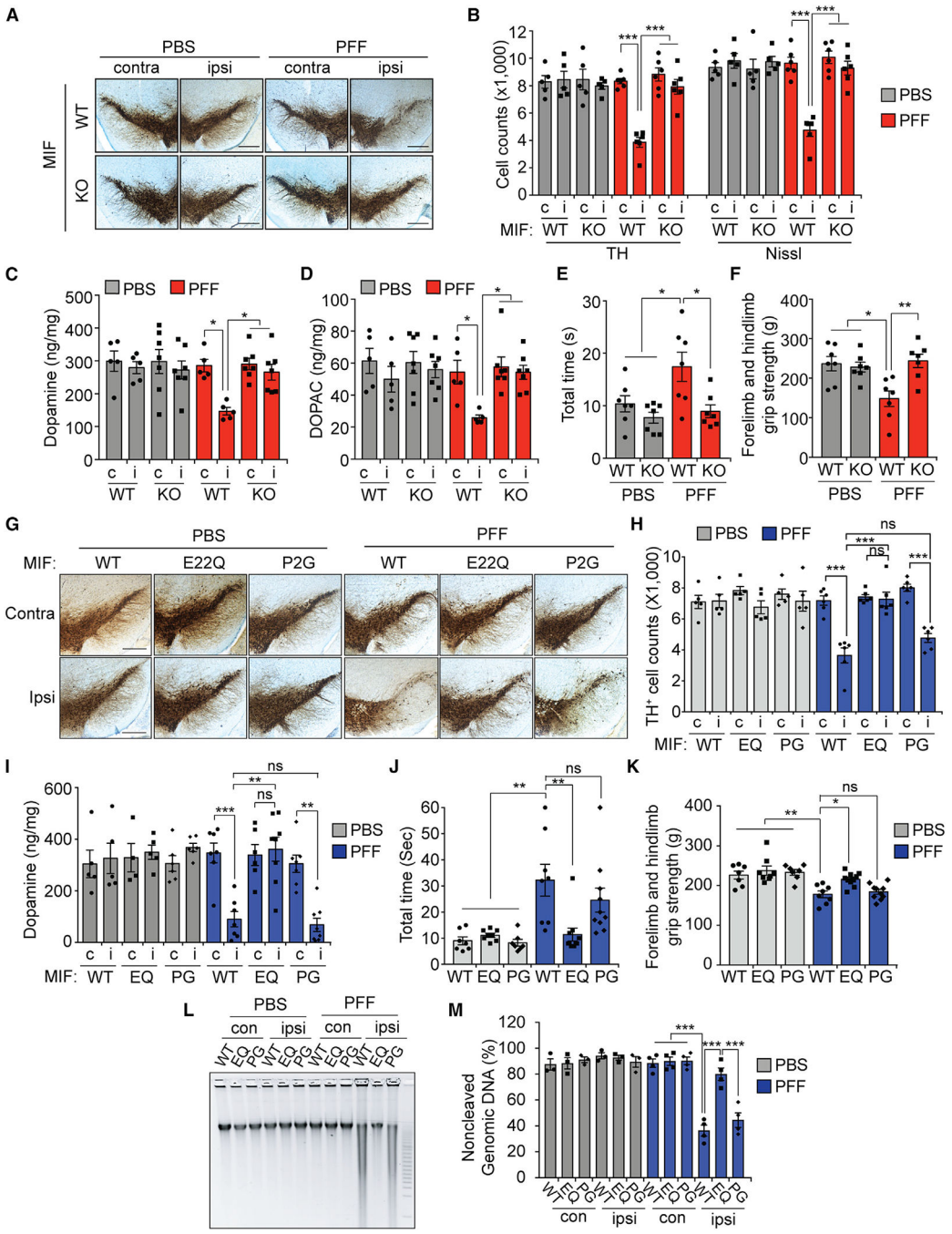

Figure 1. α-Syn PFF-induced pathology is reduced by deletion of PAAN/MIF's nuclease *in vivo*

(A) Representative TH and Nissl staining of SNpc DA neurons of α-syn PFF injected WT and PAAN/MIF KO at 6 months after α-syn PFF or PBS injection. Scale bars, 400 μm.

(B) Stereological counts of TH^+ cells. Data are mean ± SEM. ***p < 0.0005, two-way ANOVA followed by Tukey's post hoc test (n = 5–6 mice per group).

(C and D) (C) Dopamine and (D) DOPAC concentrations in the striatum of WT and PAAN/MIF KO at 6 months after α-syn PFF or PBS injection measured by HPLC. Bars

represent mean ± SEM. *p < 0.05, two-way ANOVA followed by Tukey's post hoc test (n = 5–7 mice per group).

(E and F) 180 days after intrastriatal α-syn PBS or PFF injection, (E) pole test and (F) grip strength test was performed in WT or PAAN/MIF KO. Data are the mean ± SEM. *p < 0.05, **p < 0.005, two-way ANOVA followed by Tukey's post hoc test (n = 7 mice per group).

(G) Representative TH and Nissl staining of SNpc DA neurons of WT, E22Q, and P2G knockin mice at 6 months after intrastriatal α-syn PFF or PBS injection. Scale bars, 400 μm.

(H) Stereological counts of TH^+ cells. Data are mean ± SEM. ***p < 0.0005, two-way ANOVA followed by Tukey's post hoc test (n = 5–6 mice per group). ns, not significant.

(I) Dopamine concentrations in the striatum of PAAN/MIF WT, E22Q, and P2G knockin mice at 6 months after α-syn PFF or PBS injection measured by HPLC. Bars represent mean ± SEM. **p < 0.005, ***p < 0.0005, two-way ANOVA followed by Tukey's post hoc test (n = 5–8 mice per group). ns, not significant.

(J and K) 180 days after intrastriatal PBS or α-syn PFF injection in PAAN/MIF WT, E22Q, and P2G knockin mice, (J) pole test and (K) grip strength test was performed. Data are the mean ± SEM. *p < 0.05, **p < 0.005, two-way ANOVA followed by Tukey's post hoc test (n = 7–10 mice per group).

(L) Pulsed-field gel electrophoresis in the substantia nigra of PBS or α-syn-PFF-injected PAAN/MIF WT, E22Q KI, or P2G KI mice at 6 months.

(M) Intensity of noncleaved genomic DNA is shown in the graph. ***p < 0.0005, two-way ANOVA followed by Tukey's post hoc test (n = 3–4 mice per group).

See also Figures S1 and S2.

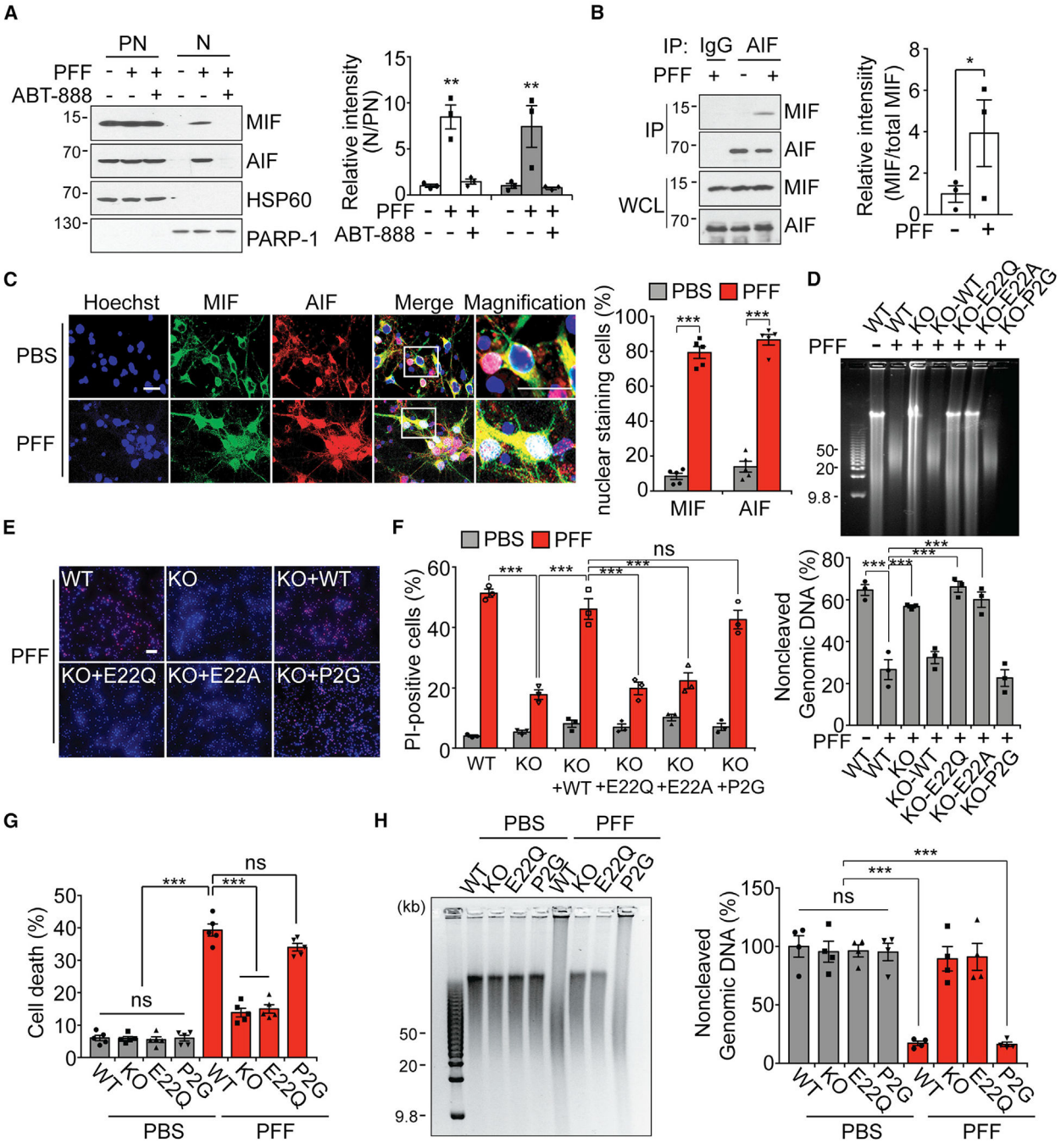

Figure 2. PAAN/MIF nuclease activity is required for prevention of α-syn PFF-induced neurotoxicity in neurons

(A) Nuclear translocation of AIF and PAAN/MIF after α-syn PFF treatment in the presence of the PARP inhibitor, ABT-888 (1 μM) in cortical neurons. Intensity of PAAN/MIF and AIF signal is shown in the graph. **p < 0.005 versus the PBS control group in the nuclear (N) fraction, two-way ANOVA followed by Tukey's post hoc test (n = 3).

(B) Immunoprecipitation (IP) of PAAN/MIF and AIF in PBS or α-syn-PFF-treated cortical neurons. Intensity of AIF-bound PAAN/MIF is shown in the graph. *p < 0.05, Student's t test (n = 3).

(C) Confocal images of nuclear translocation of PAAN/MIF (green) and AIF (red) after α-syn PFF treatment in primary cortical neurons. Scale bars, 20 μm. The white color in the merged images indicates the overlay of AIF, PAAN/MIF, and Hoechst dye in the nucleus. The percentage of cells with nuclear localization of PAAN/MIF and AIF is shown in the graph. ***p < 0.0005, Student's t test (n = 5).

(D) Pulsed-field gel electrophoresis of α-syn PFF-induced DNA cleavage in PAAN/MIF WT and KO neurons and KO neurons expressing PAAN/MIF WT, E22Q, E22A, or P2G. Intensity of noncleaved genomic DNA is shown in the graph. ***p < 0.0005, two-way ANOVA (n = 3).

(E) Representative images of Hoechst and propidium iodide (PI) staining from primary cortical neurons transduced with lentivirus containing PAAN/MIF WT, E22Q, E22A, or P2G and further incubated with α-syn PFF. Scale bars, 20 μm.

(F) Quantification of cell death. Bars represent mean ± SEM. ***p < 0.0005, two-way ANOVA followed by Tukey's post hoc test (n = 3).

(G) Quantification of cell death from Hoechst and PI staining of primary cortical neurons from PAAN/MIF WT, KO, E22Q, and P2G KI mice. Bars represent mean ± SEM. ***p < 0.0005, two-way ANOVA followed by Tukey's post hoc test (n = 5).

(H) Pulsed-field gel electrophoresis of α-syn PFF-induced DNA cleavage in PAAN/MIF WT, KO, E22Q, and P2G KI neurons treated with PBS or α-syn PFF. Intensity of noncleaved genomic DNA is shown in the graph. ***p < 0.0005, two-way ANOVA followed by Tukey's post hoc test (n = 4).

See also Figure S3

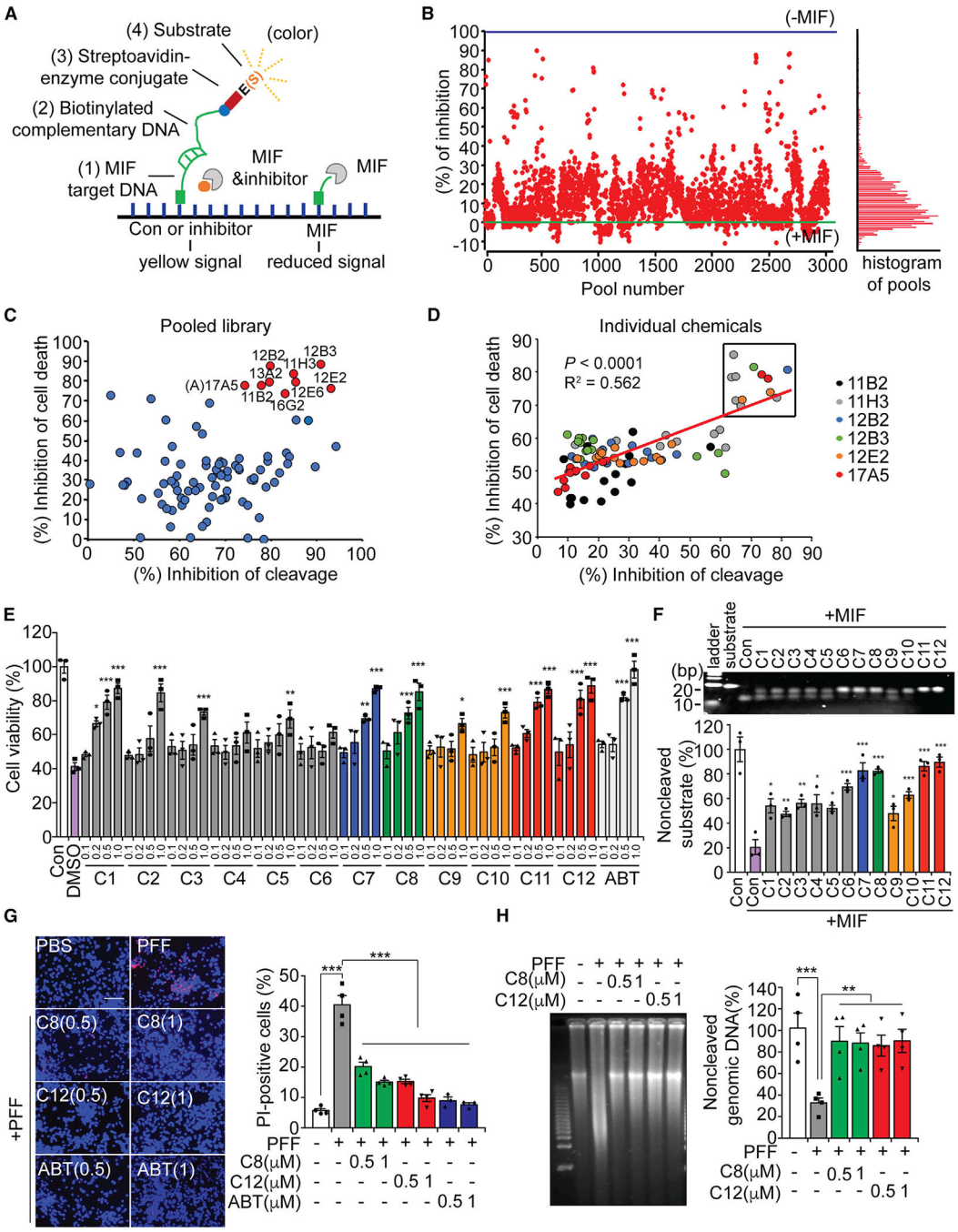

Figure 3. Identification of PAAN/MIF nuclease inhibitors

(A) The schematic representation of macrocyclic screening of PAAN/MIF inhibitors based on PAAN/MIF nuclease DNA cleavage assay. Single-strand-amino-modified oligonucleotide (RF substrate) was immobilized on DNA-BIND plates and incubated in PAAN/MIF nuclease with or without inhibitors. After PAAN/MIF's cleavage, the fragments were hybridized with biotin-labeled complementary oligonucleotides and detected by monitoring absorbance at 450 nm.

(B) Scatter plot of percentage inhibition of PAAN/MIF cleavage from 45,000 compounds with 3,000 pools in 38 plates of the macrocyclic library. The top line (blue) is the incubation without PAAN/MIF and bottom line (green) is the incubation with PAAN/MIF. Right graph represents the histogram of the compounds tested.

(C) The result of secondary screening from the primary screening pools that inhibited PAAN/MIF nuclease activity by at least 60%. Scatter plot of the percentage the inhibition of PAAN/MIF nuclease activity (x axis) and the inhibition of MNNG-induced cell death (y axis).

(D) The result of the 90 individual compounds screening of 6 pools candidates from the secondary screening. Correlation analysis between the inhibition of PAAN/MIF nuclease activity and the inhibition of MNNG-induced cell death is shown in the graph.

(E) Alamar blue cell viability assay from SH-SY5Y cells pre-incubated with PAAN/MIF inhibitors (C1–C12) selected by individual screening in a concentration-dependent manner (0.1, 0.2, 0.5, and 1 μM) in response to 50-μM MNNG for 15 min. A PARP inhibitor, ABT-888 (1 μM) is used for the positive control. Bars represent mean ± SEM. **$p < 0.005$, ***$p < 0.0005$, two-way ANOVA followed by Tukey's post hoc test ($n = 3$).

(F) *In vitro* PAAN/MIF's nuclease assay with PAAN/MIF inhibitors (C1–C12) using RF substrates. Quantification of noncleaved genomic DNA. Bars represent mean ± SEM. *$p < 0.05$, **$p < 0.005$, ***$p < 0.0005$, one-way ANOVA followed by Tukey's post hoc test ($n = 3$).

(G) Representative images of Hoechst and PI staining from human cortical neurons pre-incubated with 0.5 or 1 μM of C8, C12, or ABT-888 for 1 h and further incubated with human α-syn PFF for 14 days. Scale bars, 20 μm. Quantification of cell death. Bars represent mean ± SEM. ***$p < 0.0005$, two-way ANOVA followed by Tukey's post hoc test ($n = 4$).

(H) Pulsed-field gel electrophoresis of α-syn-PFF-induced DNA cleavage in human cortical neurons treated with C8 or C12. Intensity of noncleaved genomic DNA is shown in the graph. **$p < 0.005$, ***$p < 0.0005$, two-way ANOVA ($n = 4$).

See also Figure S4

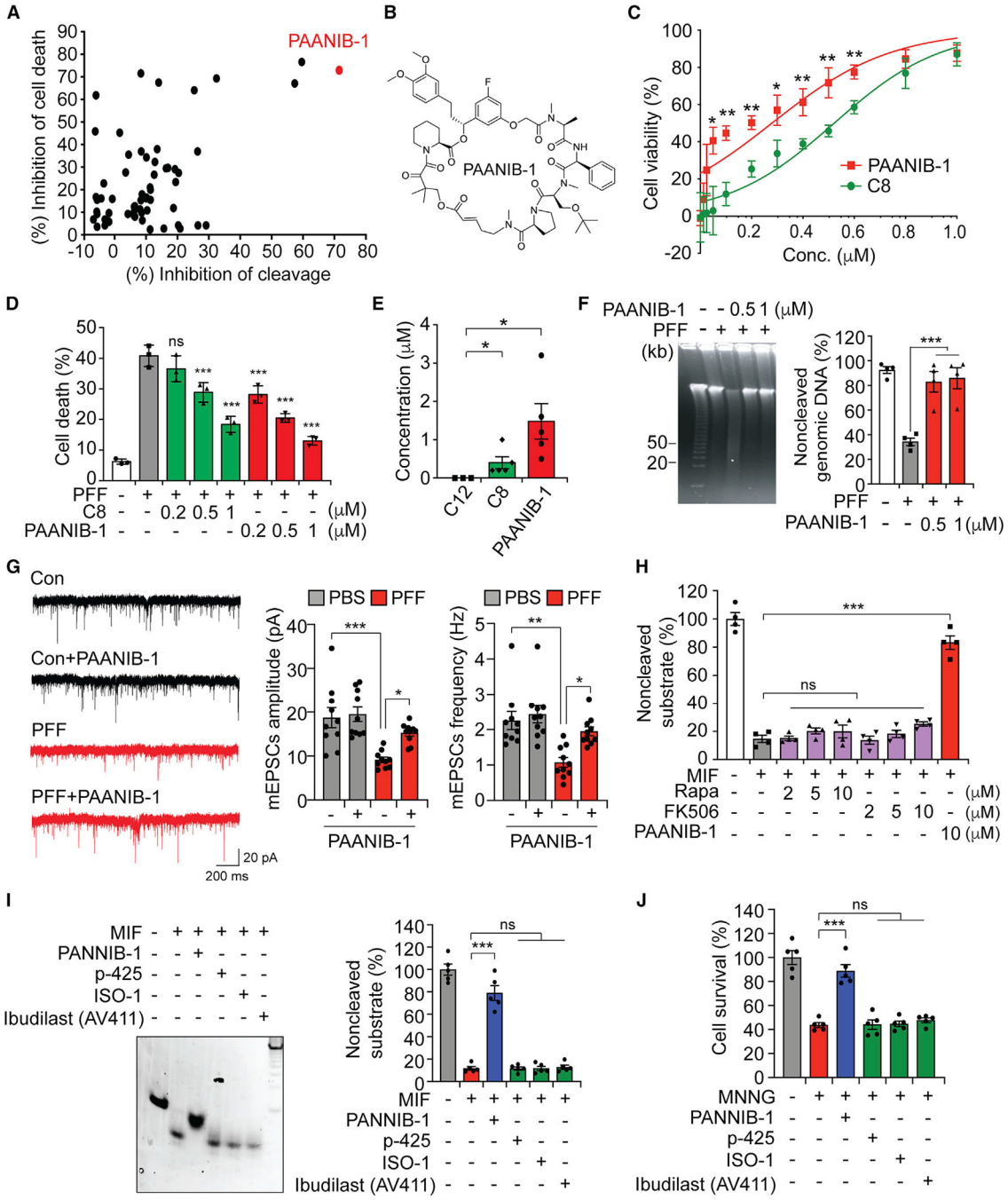

Figure 4. Identification of PAANIB-1 as a PAAN/MIF nuclease inhibitor

(A) The result of the structural-activity relationship (SAR) screening of C8. Scatter plot of the percent inhibition of PAAN/MIF nuclease activity (x axis) and the percent inhibition of MNNG-induced cell death (y axis).

(B) Structure of PAANIB-1.

(C) SH-SY5Y cells were pre-incubated C8 or PANNIB-1 with concentrations as indicated for 1 h, followed by 50-μM MNNG for 15 min. After 24 h, cell viability was measured by

Alamar blue. Data represent mean ± SEM. *p < 0.05, **p < 0.005, Student's t test (n = 3). The half maximal inhibitory concentration (IC_{50}) of C8 is 0.52 μM, and C8–31 is 0.28 μM.
(D) Quantification of cell death from Hoechst and PI staining from primary cortical neurons pretreated with 0.2, 0.5, and 1 μM of C8 or PAANIB-1, followed by further incubation with α-syn PFF. Bars represent mean ± SEM. ***p < 0.0005, two-way ANOVA followed by Tukey's post hoc test (n = 3). ns, not significant.
(E) C57BL/6 mice were orally administrated with vehicle or 10 mg/kg of C8, C12, or PAANIB-1 for 2 h. The concentrations of compounds in brain tissue were measured by LC/MS. *p < 0.05, one-way ANOVA followed by Tukey's post hoc test (n = 3–5 per group).
(F) Pulsed-field gel electrophoresis of α-syn PFF-induced DNA cleavage in mouse cortical neurons treated with PAANIB-1. Intensity of noncleaved genomic DNA is shown in the graph. Bars represent mean ± SEM. *p < 0.05, **p < 0.005, ***p < 0.0005, two-way ANOVA followed by Tukey's post hoc test (n = 4).
(G) Representative traces of mEPSCs. Primary cortical neurons were pretreated with 1 μM of PAANIB-1, followed by further incubation with α-syn PFF. After 14 days, mEPSCs were recorded in the presence of TTX (0.25 μM), bicuculline (10 μM), and APV (20 μM). Quantification of amplitude and frequency for recordings. Bars represent mean ± SEM. *p < 0.05, **p < 0.005. ***p < 0.0005, two-way ANOVA followed by Tukey's post hoc test. For each group, 10 neurons from three independent cultures were recorded and analyzed.
(H) Quantification of noncleaved substrate DNA from *in vitro* MIF's nuclease assay with indicated dose of rapamycin, FK506, or PAANIB-1 using the PS30 substrate. Bars represent mean ± SEM. ***p < 0.0005, two-way ANOVA followed by Tukey's post hoc test (n = 4).
(I) *In vitro* PAAN/MIF's nuclease assay using MIF tautomerase inhibitors (10 μM of p-425, 50 μM of ISO-1, or 10 μM of AV411) or a 10 μM of PAAN/MIF nuclease inhibitor, PANNIB-1. Quantification of noncleaved substrate DNA. Bars represent mean ± SEM. ***p < 0.0005, two-way ANOVA followed by Tukey's post hoc test (n = 5).
(J) Alamar blue cell viability assay from SH-SY5Y cells pre-incubated with PAAN/MIF tautomerase inhibitors (10 μM of p-425, 50 μM of ISO-1, or 10 μM of AV411) or 1 mM of PANNIB-1 in response to 50-μM MNNG for 15 min. Bars represent mean ± SEM. ***p < 0.0005, two-way ANOVA followed by Tukey's post hoc test (n = 5).
See also Figure S5

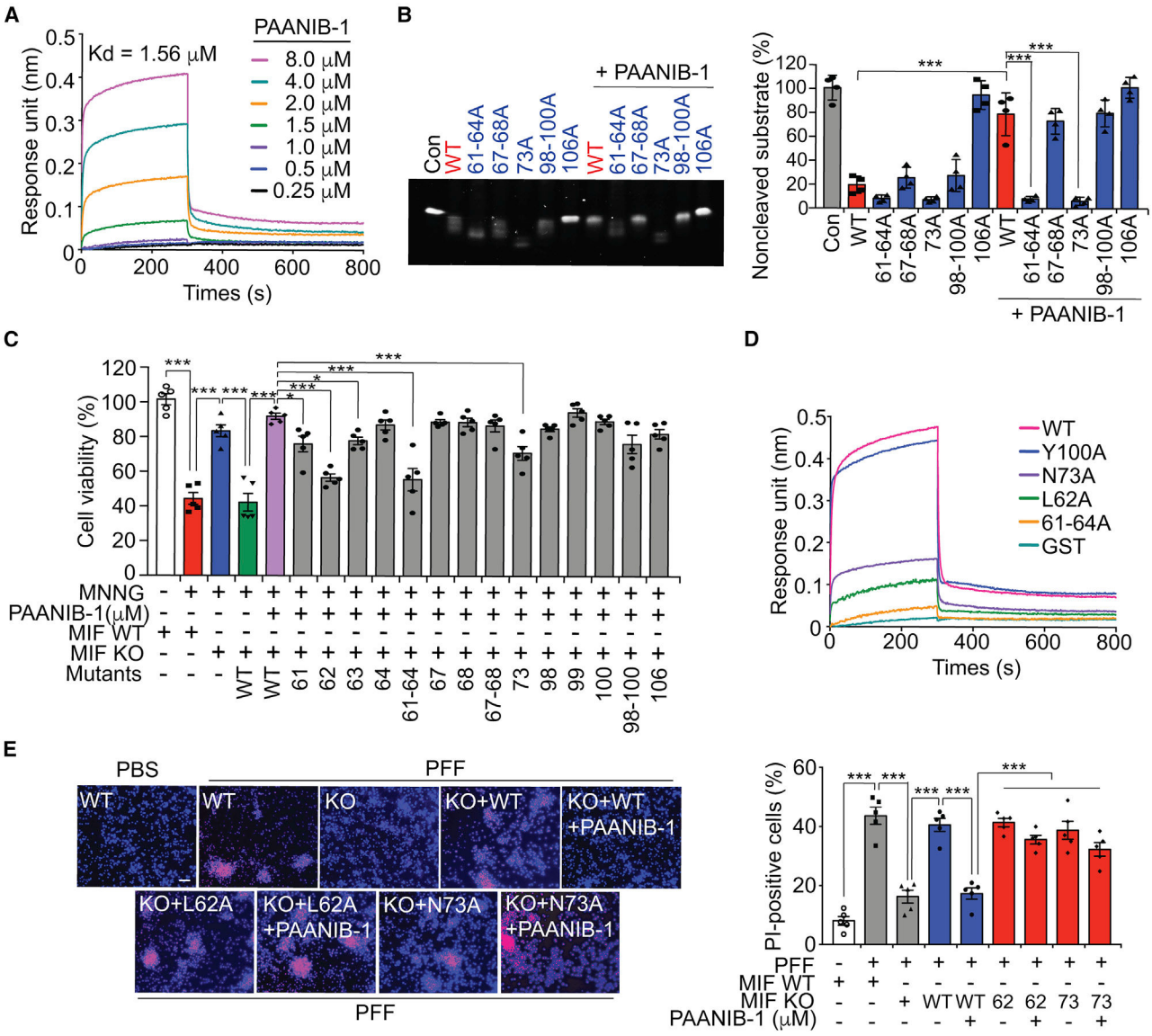

Figure 5. Direct interaction of PAANIB-1 to PAAN/MIF as an action mechanism of inhibition

(A) Binding affinities of PAAN/MIF WT for PAANIB-1 determined by biolayer interferometry (ForteBio Octet) assay. Data are representative of three independent experiments.

(B) *In vitro* PAAN/MIF's nuclease assay using PAAN/MIF WT or mutants with 10 μM of PANNIB-1. Quantification of noncleaved substrate DNA. Bars represent mean ± SEM. ***p < 0.0005, two-way ANOVA followed by Tukey's post hoc test (n = 4).

(C) WT or PAAN/MIF KO SH-SY5Y cells expressing Flag-PAAN/MIF WT or mutants were pre-incubated 1 μM of PANNIB-1 for 1 h, followed by 50-μM MNNG for 15 min. After 24 h, cell viability was measured by Alamar blue. Data represent mean ± SEM. *p < 0.05, ***p < 0.0005, two-way ANOVA followed by Tukey's post hoc test (n = 5).

(D) Binding of PAAN/MIF WT or mutants for PANNIB-1 determined by biolayer interferometry (ForteBio Octet) assay. Data are average of three independent experiments.

(E) Representative images of Hoechst and PI staining from WT or PAAN/MIF KO cortical neurons expressing PAAN/MIF WT, L62A, or N73A pre-incubated withPAANIB-1 and further incubated with α-syn PFF for 14 days. Scale bars, 20 μm. Quantification of cell death. Bars represent mean ± SEM. ***$p < 0.0005$, two-way ANOVA followed by Tukey's post hoc test ($n = 5$).
See also Figure S6.

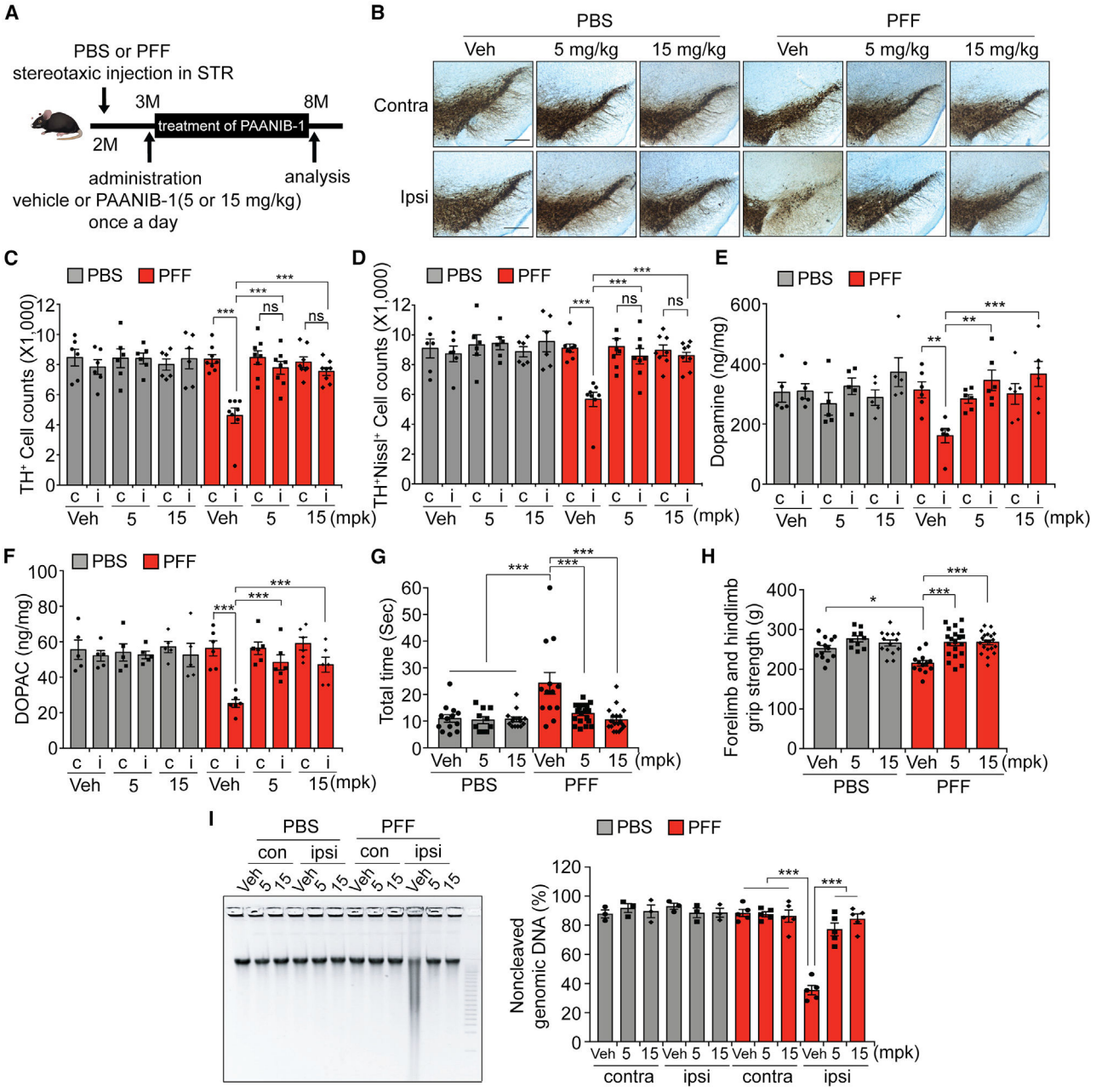

Figure 6. PAANIB-1 protects against α-syn PFF-induced pathology *in vivo*

(A) Schematic diagram of the experimental design. PBS or α-syn PFF were injected into the striatum of 2-month-old WT mice. After 1 month, PAANIB-1 or vehicle was delivered by oral administration with two different doses (5 or 15 mg/kg) for 5 months.

(B) Representative TH and Nissl staining of SNpc DA neurons of PBS or α-syn-PFF-injected WT mice treated with vehicle or PAANIB-1. Scale bars, 400 μm.

(C and D) Stereological counts of (C) TH-positive cells and (D) Nissl-positive cells. Data are mean ± SEM. ***p < 0.0005, two-way ANOVA followed by Tukey's post hoc test (n = 6–8 mice per group).

(E and F) (E) Dopamine and (F) DOPAC concentrations in the striatum of PBS or α-syn-PFF-injected WT mice treated with vehicle of PAANIB-1 as assessed by HPLC. Bars represent mean ± SEM. **p < 0.005, ***p < 0.0005, two-way ANOVA followed by Tukey's post hoc test (n = 5–6 mice per group).

(G and H) 180 days after intrastriatal α-syn PFF or PBS injection in WT mice treated with vehicle or PAANIB-1, (G) pole test and (H) grip strength test was performed. Data are the mean ± SEM. *p < 0.05, ***p < 0.0005, two-way ANOVA.

(I) Pulsed-field gel electrophoresis in the substantia nigra of PBS or α-syn-PFF-injected WT mice treated with vehicle or PAANIB-1. Intensity of noncleaved genomic DNA is shown in the graph. ***p < 0.0005, two-way ANOVA followed by Tukey's post hoc test (n = 3 to 5 mice per group).

See also Figure S7.

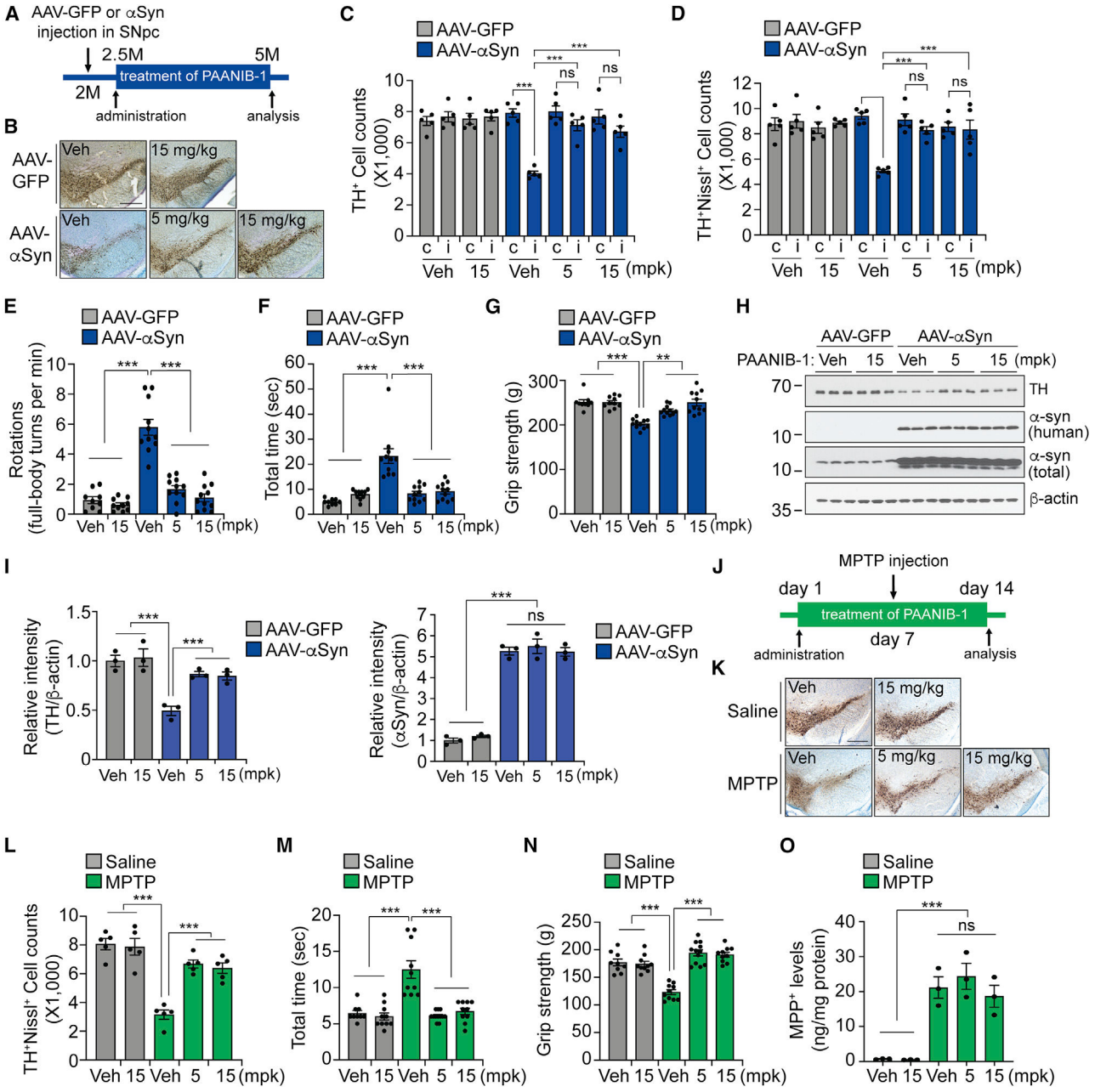

Figure 7. PAANIB-1 protects against AAV-α-syn- or MPTP-induced pathology *in vivo*

(A) Schematic diagram of the experimental design. AAV-GFP or AAV-α-syn were injected into the substantia nigra of 2-month-old WT mice. After 14 days, PAANIB-1 or vehicle was delivered by oral administration with two different doses (5 or 15 mg/kg) for 2.5 months.

(B) Representative TH and Nissl staining of SNpc DA neurons of AAV-GFP or AAV-α-syn injected WT mice treated with vehicle or PAANIB-1. Scale bars, 400 μm.

(C and D) Stereological counts of (C) TH-positive and (D) TH- and Nissl-positive cells. Data are mean ± SEM. ***p < 0.0005, two-way ANOVA followed by Tukey's post hoc test (n = 5).

(E–G) 90 days after intrastriatal AAV-GFP or AAV-α-syn injection in WT mice treated with vehicle or PAANIB-1, (E) amphetamine rotation test, (F) pole test, and (G) grip strength test was performed. Data are the mean ± SEM. **p < 0.005, ***p < 0.0005, two-way ANOVA followed by Tukey's post hoc test.

(H and I) Representative immunoblots of TH, α-syn and β-actin in SNpc of AAV-GFP or AAV-α-syn-injected WT mice treated with vehicle or PAANIB-1. Quantification of TH levels (left) and α-syn level (right) normalized to β-actin. Bars represent the mean ± SEM. ***p < 0.0005, two-way ANOVA followed by Tukey's post hoc test (n = 3). ns, not significant.

(J) Schematic diagram of the experimental design. Mice were pretreated with vehicle or PAANIB-1 (5 or 15 mg/kg) a week before MPTP injections and treatmentwas continued until experiments.

(K) Representative TH and Nissl staining of SNpc DA neurons of saline or MPTP injected WT mice treated with vehicle or PAANIB-1. Scale bars, 400 μm.

(L) Stereological counts of TH- and Nissl-positive cells. Data are mean ± SEM. ***p < 0.0005, two-way ANOVA followed by Tukey's post hoc test (n = 5).

(M and N) 7 days after saline or MPTP injection, (M) pole and (N) grip strength tests were performed. Data are the mean ± SEM. ***p < 0.0005, two-way ANOVA followed by Tukey's post hoc test.

(O) Striatal MPP^+ concentrations after a single injection of saline or MPTP treated with vehicle or PAANIB-1.

KEY RESOURCES TABLE

REAGENT or RESOURCE	SOURCE	IDENTIFIER
Antibodies		
PAR	Kam et al., 2018	N/A
Mouse monoclonal anti-PARP-1 (clone 42/PARP) antibody	BD Bioscience	Cat# 611039; AB_398352
Rabbit polyclonal anti-PAAN/MIF antibody	Abcam	Cat# 7207; AB_305760
Mouse monoclonal anti (E-1) AIF antibody	Santa Cruz	Cat# 13116; AB_626654
Mouse monoclonal anti-Flag (clone M1) antibody	Sigma	Cat# F3040; AB_439712
Rabbit polyclonal anti-phospho-S6K (Thr389) antibody	Cell Signaling	Cat# 9205; AB_330944
Rabbit monoclonal anti-p70S6 kinase (49D7) antibody	Cell Signaling	Cat# 2708; AB_390722
Rabbit polyclonal anti-phospho-S6 (Ser240/244) ribosomal protein antibody	Cell Signaling	Cat# 2215; AB_331682
Rabbit monoclonal anti-S6 ribosomal protein (clone 5G10) antibody	Cell Signaling	Cat# 2217; AB_331355
Rabbit monoclonal anti-phospho-4E-BP1 (Thr37/46) (236B4) antibody	Cell Signaling	Cat# 2855; AB_560835
Rabbit monoclonal anti-4E-BP1 (clone 53H11) antibody	Cell Signaling	Cat# 9644; AB_2097841
Rabbit polyclonal anti-Tyrosine Hydroxylase antibody	Novus Biologicals	Cat# NB300-109; AB_10077691
Rabbit monoclonal anti-Dopamine Transporter antibody	Sigma	Cat# D60944; AB_1840807
Mouse monoclonal anti-β-actin-peroxidase (clone AC-15) antibody	Sigma	Cat# A3854; AB_262011
Rabbit monoclonal anti-FKBP12 antibody	Santa Cruz	Cat# sc133067; AB_2102847
Rabbit monoclonal anti-FKBP52 antibody	Abcam	Cat# ab230952
Mouse monoclonal anti-α-synuclein phosphor(Ser129) antibody	Biolegend	Cat# 825701; AB_2564891
Rabbit monoclonal anti-α-synuclein phosphor(Ser129) antibody (D1R1R)	Cell Signaling	Cat# 23706; AB_2798868
Mouse monoclonal anti-α-synuclein antibody	BD Bioscience	Cat# 610787; AB_398107
Mouse monoclonal anti-α-synuclein antibody (Syn211)	Sigma	Cat# S5566; AB_261528
Rabbit monoclonal anti-Histone H3 (D1H2) antibody	Cell Signaling	Cat# 4499;AB_10544537
Rabbit polyclonal anti-HSP60 (D307) antibody	Cell Signaling	Cat# 4870;AB_2295614
Goat anti-rabbit IgG (H+L) Secondary antibody Alexa Fluor 488 antibody	Cell Signaling	Cat# 4412; AB_1904025
Goat anti-mouse IgG (H+L) Secondary antibody Alexa Fluor 488 antibody	Cell Signaling	Cat# 4408; AB_10694704
Goat anti-mouse IgG (H+L) Secondary antibody Alexa Fluor 594 antibody	Cell Signaling	Cat# 8890; AB_2714182
Bacterial and virus strains		
AAV2-mouse PAAN/MIF-WT-Flag	Vigene Biosciences	N/A
AAV2-mouse PAAN/MIF-E22Q-Flag	Vigene Biosciences	N/A
AAV2-mouse PAAN/MIF-P2G-Flag	Vigene Biosciences	N/A
AAV2-human α-syn	Vector Biosystems	N/A
cFugw-mouse PAAN/MIF-WT-Flag	Wang et al.,2016	N/A
cFugw-mouse PAAN/MIF-E22Q-Flag	Wang et al.,2016	N/A
cFugw-mouse PAAN/MIF-P2G-Flag	Wang et al.,2016	N/A
cFugw-mouse PAAN/MIF-L62A-Flag	This paper	N/A
cFugw-mouse PAAN/MIF-N73A-Flag	This paper	N/A
Chemicals, peptides, and recombinant proteins		

REAGENT or RESOURCE	SOURCE	IDENTIFIER
SigmaFast DAB peroxidase substrate	Sigma-Aldrich	Cat#: D0426
Normal Goat Serum (10%)	Thermo Fisher Scientific	Cat#: 500627
PolyFect reagent	Qiagen	Cat#: 301105
ABT-888 (Veliparib)	Selleckchem	Cat#: S1004
Staurosporine	Sigma-Aldrich	Cat#: 37095
Z-VAD-FMK	Selleckchem	Cat#: S7023
Tumor Necrosis Factor α (TNFα)	Sigma-Aldrich	Cat#: T7539
Necrostatin-1 (Nec-1)	Sigma-Aldrich	Cat#: N9037
1-Methyl-3-nitro-1-nitrosoguanidine (MNNG)	Sigma-Aldrich	Wang et al., 2016
MIF antagonist, ISO-1	Sigma-Aldrich	Cat#: 475837
MIF antagonist, p425	BioVision	Cat#: 2158
Ibudilast (AV-411)	MedKoo	Cat#: 319626
NMDA antagonist, D-AP5	Abcam	Cat#: ab120003
AMPA antagonist, NBQX	Abcam	Cat#: ab120046
MPTP	Sigma-Aldrich	Cat#: 506382
Neurobasal medium	Thermo Fisher Scientific	Cat#: 21103049
B-27 Supplement (50X)	Thermo Fisher Scientific	Cat#: 17504044
L-glutamine	Thermo Fisher Scientific	Cat#: 25030149
Dulbecco's Modified Eagle Medium (DMEM)	Thermo Fisher Scientific	Cat#: 11965092
Penicillin-Streptomycin	Thermo Fisher Scientific	Cat#:15140122
Dulbecco's modified Eagle's medium/nutrient mixture F-12 (DMEM/F12	Thermo Fisher Scientific	Cat#: 11320033
knockout serum replacement	Thermo Fisher Scientific	Cat#: 10828010
nonessential amino acids	Thermo Fisher Scientific	Cat#: 11140050
2-mercaptoethanol	Thermo Fisher Scientific	Cat#: 21985023
N-2 supplement	Thermo Fisher Scientific	Cat# : 17502048
mTeSRTM1	STEMCELL Technologies	Cat#: 85850
Brain-derived neurotrophic factor (BDNF)	PeproTech	Cat#: 450-02
Glial cell line-derived neurotrophic factor (GDNF)	PeproTech	Cat#: 450-10
L-Ascorbic acid	Sigma-Aldrich	Cat#: A4403
Dibutyryl adenosine 3′,5′-monophosphate (cAMP)	Sigma-Aldrich	Cat#: 28745
Hoechst 33342, Trihydrochloride, Trihydrate	Invitrogen	Cat#: H3570
Propidium iodide (PI)	Invitrogen	Cat#: BMS500PI
AlamarBlue™ Cell Viability Reagent	Invitrogen	Cat#: DAL1025
SureBeads™ Protein G Magnetic Beads	Bio-rad	Cat#: 1614023
Horseradish peroxidase (HRP)-conjugated Streptavidin	Thermo Fisher Scientific	Cat#: N100
1-step Ultra TMB-ELISA substrate solution	Thermo Fisher Scientific	Cat#: 34028
Glutathione Sepharose 4 B	GE Healthcare	Cat#: 17-0756-01
Superdex 200 10/300GL column	GE Healthcare	Cat#: 17-5175-01
Anti-GST biosensor tips	ForteBio	Cat#: 18-5096
Recombinant human PARP-1 Enzyme	Trevigen	Cat#: 4667-50-01
NAD^+ Substrate	Trevigen	Cat#: 4670-500-01
Rapamycin	Sigma-Aldrich	Cat#: R8781

REAGENT or RESOURCE	SOURCE	IDENTIFIER
FK506	Sigma-Aldrich	Cat#: F4679
Insulin	Sigma-Aldrich	Cat#: 91077C
L-3,4 dihydroxyphenylalanine methyl ester	Sigma-Aldrich	Cat#: D1507
Sodium peroxidate	Sigma-Aldrich	Cat#: 311456
Ethidium bromide	Sigma-Aldrich	Cat#: E8751
DMSO	Sigma-Aldrich	Cat#: D2650
Proteinase K	Life Technology	Cat#: 25530049
GoTag Green Master Mix	Promega	Cat#: M7123
Directpcr Lysis Reagent (mouse tail)	Viagen Biotech	Cat#: 102-T
Critical commercial assays		
Vectastain Elite ABC-HRP kit, peroxidase	Vector Laboratories	PK-6101
QuikChange site-directed mutagenesis kit	Agilent Technologies	Cat#: 210513
Calcineurin cellular activity assay	Enzo Life Sciences	Cat#: BML-AK816-0001
NAD/NADH Assay kit	Abcam	Cat#: ab65348
Experimental models: Cell lines		
SH-SY5Y	ATCC	CRL-2266
$MIF^{-/-}$ SH-SY5Y	This paper	N/A
$FKBP12^{-/-}$ SH-SY5Y	This paper	N/A
$FKBP52^{-/-}$ SH-SY5Y	This paper	N/A
Human H1 embryonic stem cells (ESCs)	Johns Hopkins Medical Institution	N/A
Experimental models: Organisms/strains		
Mouse: C57BL/6J (WT)	The Jackson Laboratory	JAX: 000664
Mouse: PAAN/MIF^{KO}: C.129S4(B6)-*Mif*^{tm1Dvd}/J	The Jackson Laboratory	JAX: 003830
Mouse: PAAN/MIF $E22Q^{KI}$/C57BL/6	This paper	N/A
Mouse: PAAN/MIF $P2G^{KI}$: C57BL/6-*Mif*^{tm2Gfr}/Mmjax	The Jackson Laboratory	JAX: 32057
Oligonucleotides		
PAAN/MIF substrate (RF substrate)	Wang et al., 2016	TCCCAAGTAGCTGGGATTACAGGAAAAAAA
Biotin labeled PAAN/MIF complementary substrate	This paper	Biotin-TTTTTTTCCTGTAA
Exonuclease III substrate forward	This paper	GTCACCGTCATACGACTC
Exonuclease III substrate reverse	This paper	GAGTCGTATGACGGTGAC
APE1 substrate forward	This paper	GTGGCGCGGAGACTTAGAGAFATTTGGCGCGGGGAATTCC
APE1 substrate reverse	This paper	CACCGCGCCTCTGAATCTCTGTAAACCGCGCCCCTTAAGG
Genotyping: Mouse PAAN/MIF KO forward	Wang et al., 2016	CGTCCAGATCATCCTGATC
Genotyping: Mouse PAAN/MIF KO reverse	Wang et al., 2016	ATTGAACAAGATGGATTGCAC

REAGENT or RESOURCE	SOURCE	IDENTIFIER
Genotyping: Mouse PAAN/MIF E22Q KI forward	This paper	GGGAGAAATTAATAGTGTG CTCCAG
Genotyping: Mouse PAAN/MIF E22Q KI reverse	This paper	CTCAGGGACCTGCTGTGAT TG
Genotyping: Mouse PAAN/MIF P2G KI forward	This paper	AATTAACTTGGTGGGAGAG GT
Genotyping: Mouse PAAN/MIF P2G KI reverse	This paper	CAGCTGGAGTGTGGGGATT TT
gRNAs targeting MIF forward	This paper	CACCGCAGAAACCCCTCTG GCACGG
gRNAs targeting MIF forward	This paper	AAACCCGTGCCAGAGGGGT TTCTG C
gRNAs targeting FKBP12-#1 forward	This paper	CAGGTGGAAACCATCTCCC C
gRNAs targeting FKBP12-#1 reverse	This paper	GGGGAGATGGTTTCCACCT G
gRNAs targeting FKBP12-#2 forward	This paper	GGTCTGGCCGCGCTTGGGG A
gRNAs targeting FKBP12-#2 reverse	This paper	TCCCCAAGCGCGGCCAGAC C
gRNAs targeting FKBP52-#1 forward	This paper	GATGAAGGCGACCGAGAGC G
gRNAs targeting FKBP52-#1 reverse	This paper	CGCTCTCGGTCGCCTTCATC
gRNAs targeting FKBP52-#2 forward	This paper	CAGCACGCCTTCGTCCTGTT
gRNAs targeting FKBP52-#2 reverse	This paper	AACAGGACGAAGGCGTGCT G
Recombinant DNA		
pRK172-α-syn (mouse and human)	Luk et al., 2012	N/A
pGEX-6P1	GE Healthcare	N/A
pGEX-6P1-hMIF-WT	Wang et al., 2016	N/A
pGEX-6P1-hMIF-61 -64A	This paper	N/A
pGEX-6P1-hMIF-S61A	This paper	N/A
pGEX-6P1-hMIF-L62A	This paper	N/A
pGEX-6P1-hMIF-H63A	This paper	N/A
pGEX-6P1-hMIF-S64A	This paper	N/A
pGEX-6P1-hMIF-67-68A	This paper	N/A
pGEX-6P1-hMIF-K67A	This paper	N/A
pGEX-6P1-hMIF-I68A	This paper	N/A
pGEX-6P1-hMIF-N73A	This paper	N/A
pGEX-6P1-hMIF-98-100A	This paper	N/A
pGEX-6P1-hMIF-N98A	This paper	N/A
pGEX-6P1-hMIF-Y99A	This paper	N/A
pGEX-6P1-hMIF-Y100A	This paper	N/A
pGEX-6P1-hMIF-N106A	This paper	N/A
p3XFlag-CMV-14	Addgene	N/A
p3XFlag-CMV-14-hMIF-WT	This paper	N/A

REAGENT or RESOURCE	SOURCE	IDENTIFIER
p3XFlag-CMV-14-hMIF-S61A	This paper	N/A
p3XFlag-CMV-14-hMIF-L62A	This paper	N/A
p3XFlag-CMV-14-hMIF-H63A	This paper	N/A
p3XFlag-CMV-14-hMIF-S64A	This paper	N/A
p3XFlag-CMV-14-hMIF-61-64A	This paper	N/A
p3XFlag-CMV-14-hMIF-K67A	This paper	N/A
p3XFlag-CMV-14-hMIF-I68A	This paper	N/A
p3XFlag-CMV-14-hMIF-67-68A	This paper	N/A
p3XFlag-CMV-14-hMIF-N73A	This paper	N/A
p3XFlag-CMV-14-hMIF-N98A	This paper	N/A
p3XFlag-CMV-14-hMIF-Y99A	This paper	N/A
p3XFlag-CMV-14-hMIF-Y100A	This paper	N/A
p3XFlag-CMV-14-hMIF-98-100A	This paper	N/A
p3XFlag-CMV-14-hMIF-N106A	This paper	N/A
Software and algorithms		
Stereo Investigator software	MicroBright-Field	https://www.mbfbioscience.com
Axiovision 4.6 software	Carl Zeiss	https://www.micro-shop.zeiss.com
Octet data analysis software	ForteBio	https://www.sartorius.com
GraphPad Prism 7	GraphPad Software	https://www.graphpad.com/